REPORT DOCUMENTATION PAGE

AFRL-SR-AR-TR-06-0033

1. REPORT DATE *(DD-MM-YYYY)*	2. REPORT TYPE	3. DATES COVERED *(From - To)*
07/09/2005	Final Report	12/01/01 - 05/31/05

4. TITLE AND SUBTITLE
Gas Turbine Tip Region Leakage Flow and Heat Transfer

5a. CONTRACT NUMBER

5b. GRANT NUMBER
F49620-02-1-0027

5c. PROGRAM ELEMENT NUMBER

6. AUTHOR(S)
John E. LaGraff – Syracuse University

Martin Oldfield - Oxford University
Pepe Palafox - Oxford University

5d. PROJECT NUMBER

5e. TASK NUMBER

5f. WORK UNIT NUMBER

7. PERFORMING ORGANIZATION NAME(S) AND ADDRESS(ES)

Syracuse University
113 Bowne hall
Syracuse, NY 13244

8. PERFORMING ORGANIZATION REPORT NUMBER

Agreement #3531446

9. SPONSORING / MONITORING AGENCY NAME(S) AND ADDRESS(ES)
AFOSR/NA
875 N. Randolph St., Ste 325
Arlington, VA 22203-1768

10. SPONSOR/MONITOR'S ACRONYM(S)

11. SPONSOR/MONITOR'S REPORT NUMBER(S)

12. DISTRIBUTION / AVAILABILITY STATEMENT

DISTRIBUTION STATEMENT A. Approved for public release; distribution is unlimited.

13. SUPPLEMENTARY NOTES

14. ABSTRACT
New, detailed flow field measurements and high resolution Nusselt number (Nu) distributions are presented for a very large low-speed cascade representative of a high-pressure turbine rotor blade with turning of 110 degrees and blade chord of 1.0 m. Data was obtained for tip leakage and passage secondary flow at a Reynolds number of 4.0×10^5, based on exit velocity and blade axial chord. Tip clearance levels ranged from 0% to 1.68% of blade span (0% to 3% of blade chord). The relative motion between the casing and the blade tip was simulated using a motor-driven moving belt system. Particle Image Velocimetry (PIV) was used to obtain flow field maps of several planes parallel and normal to the tip surface within the tip gap, and adjacent passage flow. Secondary flow was measured at planes normal to the blade exit angle at locations upstream and downstream of the trailing edge. An infrared camera made detailed temperature measurements on a constant heat flux tip surface. The interaction between the tip leakage vortex and passage vortex is clearly defined, revealing the dominant effect of the tip leakage flow on the tip endwall secondary flow. A reduction in the magnitude of the under-tip flow near the endwall due to the moving wall is observed and the effect on the tip leakage vortex examined. The moving belt endwall significantly shifts the region of high Nu distribution and reduces the overall averaged Nu on the tip surface by up to 13.3%. The addition of a suction side squealer tip significantly reduced local tip heat transfer and resulted in a 32% reduction in averaged Nu.

15. SUBJECT TERMS
Gas turbine; tip-flow; heat transfer

16. SECURITY CLASSIFICATION OF:			17. LIMITATION OF ABSTRACT	18. NUMBER OF PAGES	19a. NAME OF RESPONSIBLE PERSON
a. REPORT unclassified	b. ABSTRACT unclassified	c. THIS PAGE unclassified	None	27	John E. LaGraff
					19b. TELEPHONE NUMBER *(include area code)* 315-443-1189

Standard Form 298 (Rev. 8-98)
Prescribed by ANSI Std. Z39.18

Gas Turbine Tip Region Leakage Flow and Heat Transfer

ABSTRACT

New, detailed flow field measurements are presented for a very large low-speed cascade representative of a high-pressure turbine rotor blade with turning of 110 degrees and blade chord of 1.0 m. Data was obtained for tip leakage and passage secondary flow at a Reynolds number of 4.0 x 10^5, based on exit velocity and blade axial chord. Tip clearance levels ranged from 0% to 1.68% of blade span (0% to 3% of blade chord). Particle Image Velocimetry (PIV) was used to obtain flow field maps of several planes parallel to the tip surface within the tip gap, and adjacent passage flow. Vector maps were also obtained for planes normal to the tip surface in the direction of the tip leakage flow. Secondary flow was measured at planes normal to the blade exit angle at locations upstream and downstream of the trailing edge. The interaction between the tip leakage vortex and passage vortex is clearly defined, revealing the dominant effect of the tip leakage flow on the tip endwall secondary flow. The relative motion between the casing and the blade tip was simulated using a motor-driven moving belt system. A reduction in the magnitude of the under-tip flow near the endwall due to the moving wall is observed and the effect on the tip leakage vortex examined.

NOMENCLATURE

Roman

AC	Alternating current
C	Blade chord
C_{ax}	Blade axial chord
CCD	Charge-coupled device
C_P	Static pressure Coefficient = $\frac{P_\infty - P}{q_\infty}$
h	Blade span,
H	Shape factor
HTC	Heat transfer coefficient
k	Thermal conductivity
LE	Leading edge
L	Tip gap length or thickness; Characteristic length
$\dot{m}$	Mass flow rate
Nu	Nusselt number
P	Static pressure
P_0	Total pressure
PIV	Particle image velocimetry
PS	Pressure side surface of blade
PV	Passage vortex
q	Dynamic pressure
R	Reattachment location
Re	Reynolds number
SB	Separation Bubble
s	Blade pitch
SS	Suction side surface of blade
SV	Scraping vortex
T	Temperature
t	Gap height
TE	Trailing edge
TLV	Tip leakage vortex
t_{max}	Maximum thickness of the blade
Tu	Turbulence intensity
TET	Turbine inlet temperature, turbine entry temperature
V	Velocity
V_{ex}	Cascade exit velocity
V_B	Belt velocity
W	Work
δ	99% boundary layer thickness
δ^*	Displacement thickness
θ	Momentum thickness

Subscripts

s	Static conditions
0	Total conditions
1	Cascade inlet conditions
2	Cascade outlet conditions
4	Upstream conditions

INTRODUCTION

In unshrouded axial flow turbines, there is necessarily a clearance between the rotating blade tips and the surrounding stationary casing, which is the cause of significant efficiency and heat transfer penalties. This gap allows passage fluid to flow from the pressure to the suction side of the blades, driven by the pressure difference across the blade. This tip leakage flow is accelerated through the gap reducing the work done on the blade, generating losses in the gap and eventually exiting on the suction side where it mixes with on-coming passage flow as it rolls up into the tip leakage vortex. An estimated 1-2% loss in turbine efficiency has been associated with a 1%Span of gap [1]. Highly-loaded turbine rotors are especially affected by this leakage flow, where in addition to efficiency losses, the high-temperature exhaust gases from the combustor and elevated heat transfer rates in the vicinity of the tip lead to the reduction of the blade's life. The casing has also been found to become more affected by these heat transfer loads over the blade tip. As pressure ratios and turbine inlet temperatures are raised in the quest for reduced fuel consumption and increased specific power, the understanding of tip flows in unshrouded turbines becomes ever more crucial. Over the past couple of decades, several studies have contributed to the general understanding of the phenomena taking place in turbines. Linear cascades have been used extensively and have been successful in providing a better understanding of the physics involved [2]. While matching the blade loading, Reynolds number and other key parameters, linear cascades have simplified the problem and allowed for larger scale cascades to provide greater detailed measurements in the many regions of the turbine. The

relative motion between the blades casing endwall is probably the most significant effect not simulated in most cascade experiments.

Early studies by Moore and Tilton [3] showed the acceleration of the flow into the tip gap and the formation of the vena contracta on the tip surface next to the pressure side. The flow subsequently experienced significant diffusion and mixing prior to exiting the gap on the suction side. In contrast to Moore and Tilton's model, where the tip leakage flow mixed fully prior to exiting the gap, Heyes and Hodson [4] put forward a model comprised of an isentropic jet and a separation bubble wake, which took into account the effect of mixing in their thinner-blade cascades. Increasing the amount of total mixing inside the tip gap increased the discharge coefficient. Also, the effect of boundary layer growth over the blade tip revealed a possible reduction effect of 5% on the discharge coefficient, thereby reducing the overall leakage loss. With micro-tapping technique, Bindon [5] studied in more detail the pressure distribution in the tip region as affected by the tip gap height. He noticed a very low pressure coefficient on the suction side of his blade, which was reduced as the clearance gap was increased. He found the lowest pressure, 2.8 times smaller than cascade outlet pressure, to occur on the pressure corner. He also found the lowest pressures to occur at 60%Chord and the pressures on the tip and endwall surfaces to increase with increasing tip gap height. In another study, Bindon [6] quantified for the first time the contributions by mixing (48%), internal gap shear (39%) and endwall/secondary flow (13%) to the overall tip clearance loss for 2.5%C tip clearance gap. Yaras and Sjolander [7], using more slender blades with lower turning angle and higher gap clearance, found that a much lower loss was generated in the gap.

Yaras et al. [8 & 9] also studied the effects of the endwall relative motion on tip gap flow, downstream flow field and blade loading by employing a motor-driven belt with thin-blades, low turning angle cascade. For a gap clearance of 3.8%C and a Re=1.4 x 10^5, they found that although the shearing affect of the moving wall on the gap flow was quite small, it led to a decrease in the pressure difference across the gap and thus a reduction in the acceleration of the tip flow. The moving wall strengthened and drew the passage vortex towards the gap flow outlet (suction side) creating a throttling affect on the gap flow, which resulted in a 50% reduction of the mass flow rate through the gap. Measurements of the flow field, taken downstream of the TE, revealed enhancement of the passage vortex and weakening of the leakage vortex with increasing belt speed. A reduction in blade loading due to the moving wall effect was only noticeable at locations very near the tip.

Yamamoto [10] looked at the interaction of the leakage flow with the passage vortex at a plane 24% C_{ax} downstream. He observed an insignificant interaction between the two vortices for a low tip clearance of t/h=1.3%, but noticed stronger interaction with increasing clearance. The stronger leakage vortex pushed the passage vortex, which became weaker, towards the pressure side of the passage. In a later paper [11], detailed velocity vectors and streaklines on a blade-to-blade plane between the endwall and tip surface as well as total pressure contours on a downstream plane were presented. These effectively showed the relationship between the tip leakage and endwall flow and cascade loss generation.

In an early heat transfer study, Mayle and Metzger [12] looked at the effect of the relative blade-casing motion on the tip heat transfer using a simple rectangular profiled stationary model with concave surface adjacent to a motor-driven, rotating disk. The effect on the heat transfer due to the relative motion was found to be negligible over a range of parameters tested. In a later study, Chyu et al. [13] also found that the relative motion had negligible effect for their simple grooved tip model. In a more recent study by Srinivasan and Goldstein [14], the heat transfer on the tip was studied in a linear cascade incorporating a moving wall apparatus with the use of naphthalene sublimation technique. Very little effect of the moving wall was found in the region near the trailing edge. However a 9% reduction on the heat transfer was found to occur at mid-chord locations for a gap of t/C=0.6%. It was speculated that the tip leakage vortex moving closer to the suction surface was the cause of this reduction. Interestingly, an increase in their measured Sherwood number was found in some regions in the upstream half of the blade. A slight increase was also found in the region near the TE for a gap of t/C=0.86% with the introduction of the moving wall. No effect due to relative motion was seen at larger clearance gaps. Other tip heat transfer studies where no relative motion has been simulated includes that of Bunker et al. [15] and Azad et al. [16] where detailed *HTC* maps on the tip surface have been provided for a range of tip clearances and two turbulence intensities. Increase in the overall heat transfer was found in both cases for increasing gap clearances and increasing turbulence intensities.

Some recent studies have also focused on studying the effect of the tip flow on the heat transfer of the adjoining casing wall. Chana and Jones [17] used thin film gauges to measure the heat transfer on the casing wall and flow adiabatic wall temperature in the gap of their QinetiQ Isentropic Light Piston Facility (ILPF) with correct non-dimensional engine conditions. The casing was shown to suffer the highest heat transfer as the rotor blades pass under it; the high heat transfer rates were attributed to the tip leakage flow. In a 2-part paper presented by Thorpe et al. [18 & 19], detailed heat transfer and pressure measurements were provided for the over-tip casing wall of their Isentropic Light Piston Tunnel, which operates at engine representative conditions. These confirmed the general results of Chana and Jones [17] that the casing heat transfer peaks as the tip passes the casing. Given the previous research studies, there is still a need for the further aerodynamic studies, with higher spatial resolution, in order to better understand the behavior of the flow in tip region and how this flow is related to the heat transfer. These studies are especially important in cascades that are representative of high-pressure turbines with relative motion simulation, where data is very scarce or non-existent.

In the present paper, the recent work being conducted at Oxford University with the use of a large-scale linear cascade with a moving belt is introduced. Details concerning the use of Particle Image Velocimetry, PIV, to provide detailed measurements in the restricted region of the tip gap are given. Initial detailed results are presented for the gap region and adjacent passage flow for the largest gap clearance studied.

EXPERIMENTAL APPARATUS AND PROCEDURES

TEST CASCADE AND TEST SECTION

In order to study of the tip leakage flow in great detail, the geometry of the cascade design used in this investigation was scaled up to a blade chord length of 1 meter. In doing so, it allows for measurements to be conducted in clearance gaps of up to 30mm height, which is equivalent to a 1.68%Span or 3%Chord. Figure 1 summarizes the cascade geometry and test conditions used in the present study. As illustrated in the figure, the cascade arrangement was set up inside an existing 2m × 4m suction type wind tunnel. In order to achieve the design turning angle, part of the wind-tunnel's left wall was removed and a new bell-mouthed inlet, which provides the inlet flow to the cascade, was set up there. The previously existing inlet to the wind tunnel was blocked off.

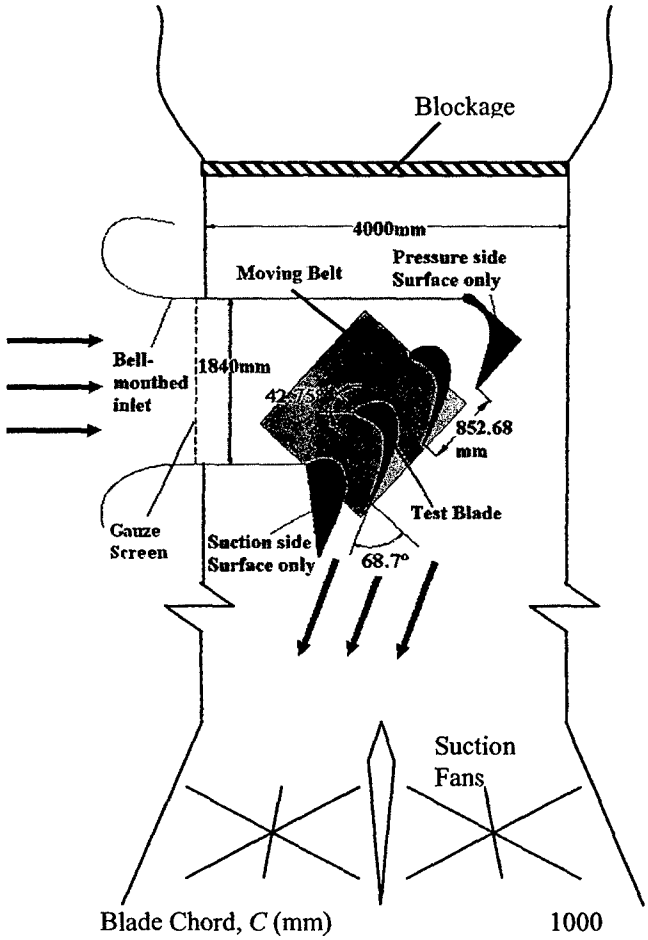

Blade Chord, C (mm)	1000
Blade Axial Chord, C_{ax} (mm)	808
Blade thickness, t_{max} (mm)	243
Blade Pitch, s (mm)	853
Design Span, h (mm)	1785.6
Actual Span (mm)	1000
Inlet Flow angle (degrees)	42.75
Blade Exit angle (degrees)	68.7
Reynolds No. (based on V_{ex} and C_{ax})	4.0×10^5

FIG 1. Cascade Geometry and Test Conditions. The cascade was mounted in an existing large wind tunnel

The blade profile and cascade geometry used was an ERCOFTAC test case comprehensively tested at Durham University by Gregory-Smith [20] for research mainly in secondary flow without tip gap. The profile of the blade is that of a high-pressure turbine with a high turning angle of 111.45°. It should be noted that actual blade span was chosen to be nearly half of the design span after smoke visualization tests revealed no interaction between the hub endwall and the tip endwall secondary flows at a 1 meter span. Two fully-profiled and two semi-profiled blade models compose the three-passage linear cascade. Passage flow measurements were conducted in the centre passage and tip-leakage flow measurements were conducted on the blade

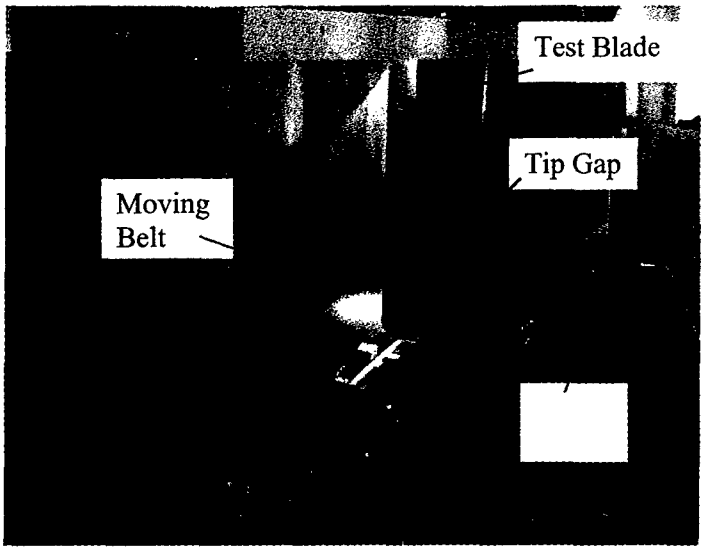

FIG. 2 Cascade test section and moving belt.

labeled test blade. The blades were made from flexible plywood, which were wrapped around profiled spars. The test blade differs from the other models in that it is mostly hollow throughout, which is an important part of the design, as will be seen in later sections, when measuring the tip flow without any interference.

The arrangement of the cascade inside the 2m × 4m wind tunnel, used to generate the appropriate conditions, is illustrated in Figure 2. As shown, the blade models were secured to a frame, which was fixed to the tunnel floor, and under the suspended blades sits a motor-driven belt system. The moving belt system and wooden boards that make up the endwall were set up on individual frames with height adjusting feet, which allow for the changing of the tip gap clearance.

The moving belt, designed to simulate the relative motion between the rotor blades and casing wall, completely covers the area under the test blade and center passage where measurements are taken. The belt extends over half an axial chord length upstream of the leading edge of the blade in order to produce a representative skewed inlet boundary layer in tests simulating the relative motion. The belt was made of a top layer of polyurethane (facing the flow) and a lower layer of polyester with a total thickness of 2mm. The belt sits on a perforated plate, which is the cover of a suction box, and is tensioned by a pair of aluminum rollers at the ends. A 7.5kW AC motor with a variable speed controller drives one of the rollers and thus drives the belt across the cascade at a constant velocity. Vertical displacements of the belt have been measured to be less than +/- 0.05mm, due to proper tensioning and suction applied by the vacuum box. The belt speed is calculated from velocity triangles and is defined as 1.34 times the inlet velocity.

The blade loading was measured at a distance of 10%*C* from the tip endwall with no gap and was compared with Durham's results (Figure 3). The profiles overlap almost perfectly, ensuring the flow conditions around the test blade are correct. A stagnation point was also measured on the blade and as expected was at the leading of the blade.

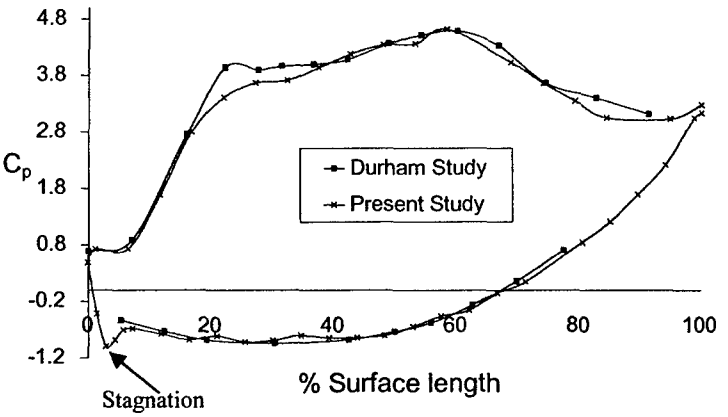

FIG 3. Blade Pressure Profile.

INSTRUMENTATION AND DATA ACQUISITION

Particle Image Velocimetry, PIV, was used to measure the flow inside and around the gap region, as well as secondary flow, with and without tip gap. The components of this PIV system were: water-based glycerin particles (introduced into the upstream flow by atomizers), the Nd: YAG laser, which was used to illuminate the flow, the CCD camera, which captured successive pairs of particle maps at a rate of 15Hz, PIV 2000 processor, used to correlate vector maps from the pairs of particle images, and the FlowMap

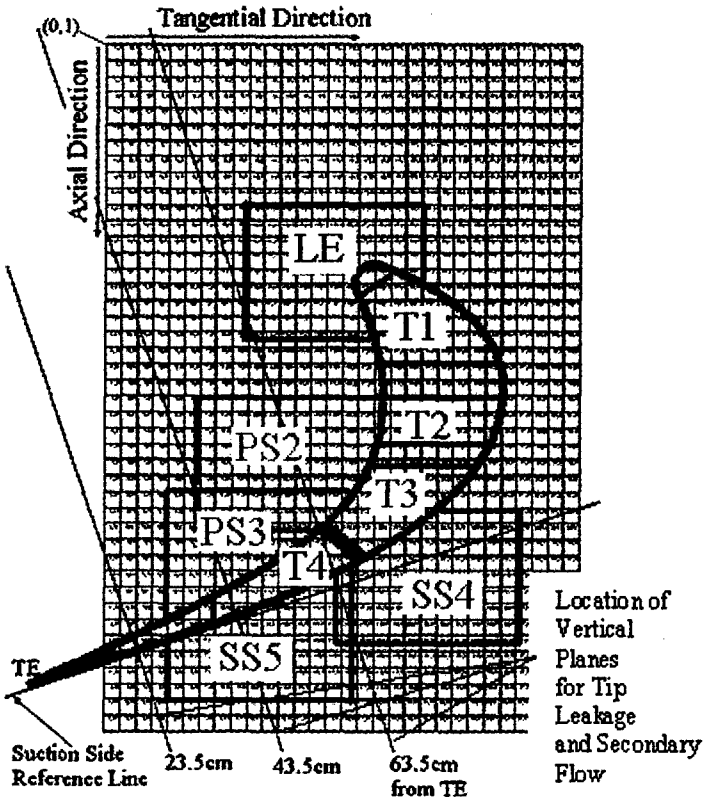

FIG. 4 Grid for Mapping Tip leakage and Secondary flow. Note the blade material is that shaded in brown.

software (on the PC), which allows user interface and post-processing of data. For each test, a total 150 pairs of instantaneous vector maps were generated and these 10 seconds worth of data were averaged to give the mean flow results presented in this paper. Except for the four maps at the end, the instantaneous, unsteady flow results will be presented in a future paper.

Particle Image Velocimetry, PIV, [21] measures fluid flow fields by tracking the movement of particles seeded into the fluid. The flow is seeded with particles and pairs of laser pulses separated in time illuminate a thin plane in the flow. A camera, placed at right angles to the sheet, captures frozen images of particles at two closely spaced instants in time. Each pair of successive images is then cross-correlated to obtain the displacement of the particles. With the time interval between successive pulses known, velocities for each particle are computed, thus generating vector maps. It is important to know that each vector generated pertains to an area of pixels, known as an interrogation area, from which the average displacement of the particles tracked in that area is measured. Typical interrogation areas are 16x 16, 32 x 32, 64 x 64 and 128 x 128 pixels.

Given the scale of the geometry, a large gird, which extends 900mm in the tangential direction and 1290mm in the axial direction, was used to map out the flow measured in specific planes (Figure 4). The grid allows for the alignment and placement of the PIV laser sheet and CCD camera in defined locations with reference to the test blade, as well as providing a scale factor needed for the calculation of velocities of particles.

There were essentially two types of measurement planes in these experiments, horizontal planes, which were parallel to the tip and endwall surface, and vertical planes, which were normal to the tip and endwall surface. The main objective of this study is to provide detailed three-dimensional flow field maps of the flow within and in the vicinity of the tip gap. This is accomplished by setting up the PIV laser sheet parallel to the tip surface (Figure 5a) and taking measurements at several distances from the endwall surface. As shown in the figure, the CCD camera can be positioned either inside the blade or on top of the blade, at right angle to the laser sheet. For the current measurements, the camera has been positioned on top of the blade, where it sits on a thick Perspex sheet, which supports the test blade and acts as the hub endwall. Measurements were taken at a range of distances from 3mm to 27mm from the endwall with increments of 3mm, i.e. 3mm, 6mm, 9mm, etc. So, the planes located at 3mm are the closest to the endwall surface and planes at 27mm are the closest to the tip surface. As mentioned previously, due to the scale of the cascade, the parallel planes are broken up into smaller planes, which include a LE plane, 5 PS planes, 5 SS planes and 4 tip planes (Figure 4). Eventually all the individual flow fields were amalgamated into single planes at a known distance from the endwall. Note that in plane T4 (plane in the aft part of the blade) in Figure 4 that the flow field near the trailing edge of the blade cannot be measured as the blade structure obscures the view. Also, since the area near the trailing edge is narrower, the smaller area of flow field seen by

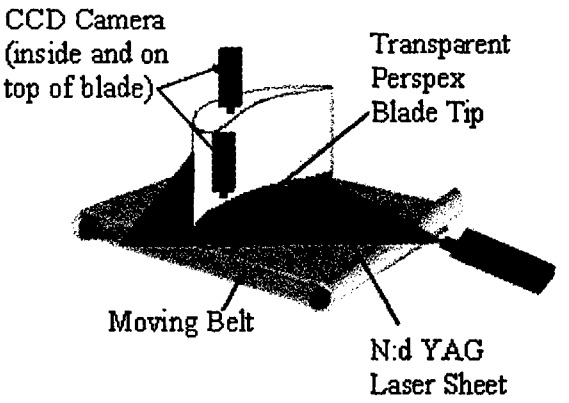

(a) Planes parallel to tip surface, within the tip gap height.

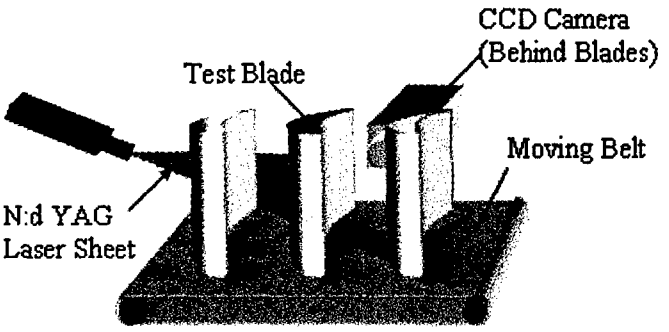

(b) Planes normal to tip surface, within the tip gap height, and secondary flow planes.

FIG. 5 PIV instrumentation setup.

the camera produces weaker correlations, which are not included in the results presented here.

Measurements in the vertical planes, as shown in Figure 5b, were taken by having the laser sheet aimed at the suction side of the blade, illuminating a slice of the passage flow and a slice of the tip leakage flow, and the CCD camera looking at the flow illuminated by the laser sheet at a location downstream of the cascade. As shown on the grid map in Figure 4, these planes are at three locations normal to the suction reference line, which is a line extending from the straight part of the suction surface near the TE, and specified distances from the TE. These planes are the same for both tip leakage flow measurements and secondary flow measurement for the purpose of seeing the development of the flow as it passes through the tip gap and emerges into the passage flow. The location of these planes is essentially in the aft part of the blade, mainly because of the physical obstruction of the adjacent blade on the laser sheet in the case of planes further upstream. However, it is known that the flow in the aft part of the blade that is of most interest.

EXPERIMENTAL RESULTS

Table 1. Boundary Layer Properties 1 chord length upstream of LE

99% Boundary Layer Thickness, δ(mm)	40.0
Displacement Thickness, δ^*(mm)	6.53
Momentum Thickness, θ(mm)	4.14
Shape Factor, H	1.57
Turbulence Intensity, Tu %	1.2

SMOKE VISULIZATION

Smoke visualization was carried out in order to get a general idea of the behavior the flow in this arrangement. Initial smoke visualization experiments were done with zero gap clearance and no moving wall, where the tip endwall surface was essentially made up of wooden boards. In these experiments, the formation of the horseshoe vortex at the blade leading edge and the passage vortex, as well as the separation of the flow on the blade suction surface were clearly seen.

Smoke visualization tests were then conducted with a tip gap of 0.58%Span (or 1%Chord). These tests revealed where and to what extent the passage flow near the gap on the pressure side was sucked into the gap. This gave a good indication of favorable locations of where to seed particles for the PIV experiments, which followed. More interestingly, clear visualizations of the tip leakage and passage vortex interaction were obtained (Figure 6). The superior strength of the tip leakage vortex, TLV, is clearly noticeable.

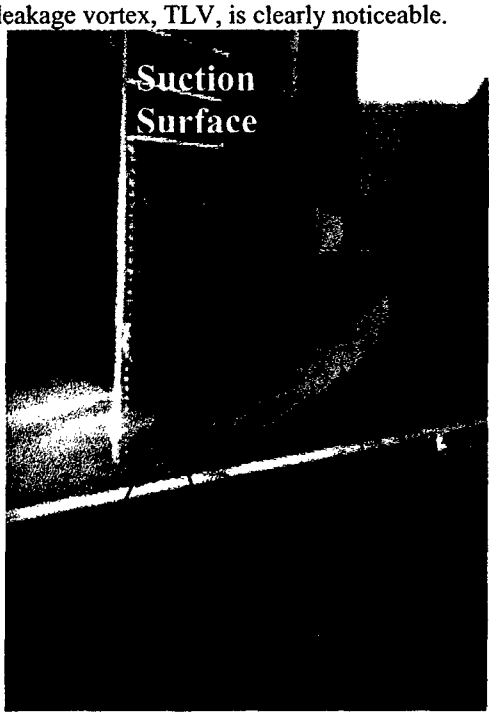

FIG. 6 Smoke Visualization of Tip Leakage Vortex and Passage Vortex Interaction for t/h=0.58%, No Moving Belt.

When compared to the images obtained with no tip gap, it was clearly seen that tip leakage vortex reduces the size of the passage vortex, PV, and shifts it closer to the suction side. These tests also revealed no interaction between the hub endwall and tip endwall secondary flows, as seen from the figure that the passage vortex on the tip endwall side of the blade does not even reach the height of 40% actual span.

SECONDARY FLOW MEASUREMENTS

Secondary flow measurements were taken at three locations and for three scenarios: 1) no tip gap, 2) with tip gap but no relative endwall motion, and 3) with tip gap and with relative endwall motion. Results are displayed in the form of vector maps overlapped with a color map of scalar magnitudes, which are divided by the cascade exit velocity, in order to see the strength of the flow. The reader should be aware that since that the camera sees the flow on the plane normal to the suction side reference line from a position downstream of the cascade, flow near the suction side is not seen by the camera as the curvature of the blade produces an obstruction, especially at planes further upstream (refer to Figure 4). These blank regions are presented as white areas with no vectors. Only the results obtained at the plane 63.5cm from the TE are presented in this paper.

Secondary flow measurements were conducted with no tip gap in order to see how the flow changes with the introduction of a gap clearance and moving endwall surface. The measured passage vortex is displayed in Figure 7. As expected, the pressure gradients in the passage create a cross flow going from the pressure side of one blade to the suction side of the adjacent blade. As the cross flow encounters the suction side surface, it rolls up into the passage vortex.

Figure 8 displays the secondary flow for a clearance gap of 1.68% Span with no relative endwall motion. The reader is advised that the flow up to 10mm from the endwall is not presented, as it cannot be measured because of laser reflections on the endwall surface. Nevertheless, the jet of high velocity emerging from the tip gap is clearly seen in the lower part of the TLV. The high velocity jet extends as far as 125mm from the suction side reference line before it is turned in the vertical direction and magnitude of the velocity decreases slightly to become the outer region of constant velocity, which goes around the core of the vortex. In comparison to the case of no tip gap, the effect of the TLV on the PV is clear. The TLV shifts the core of the PV upward by about twice the original distance from the endwall. In contrast to the case of no gap, where the PV has a definite circular, vortical shape, the presence of the TLV distorts its shape and weakens it. In the gap case, it is clear that the TLV is significantly stronger than the PV, confirming the importance of the TLV on the passage flow.

With relative endwall motion, as was observed by Yaras and Sjolander [9] the TLV moves towards the suction sides of the passage (Figure 9), partly blocking the tip gap exit. Interestingly, the jet velocity seems to have the same magnitude as in the case of no relative endwall motion. However, the belt boundary layer forces itself under the leakage jet and diverts the flow in the vertical direction.

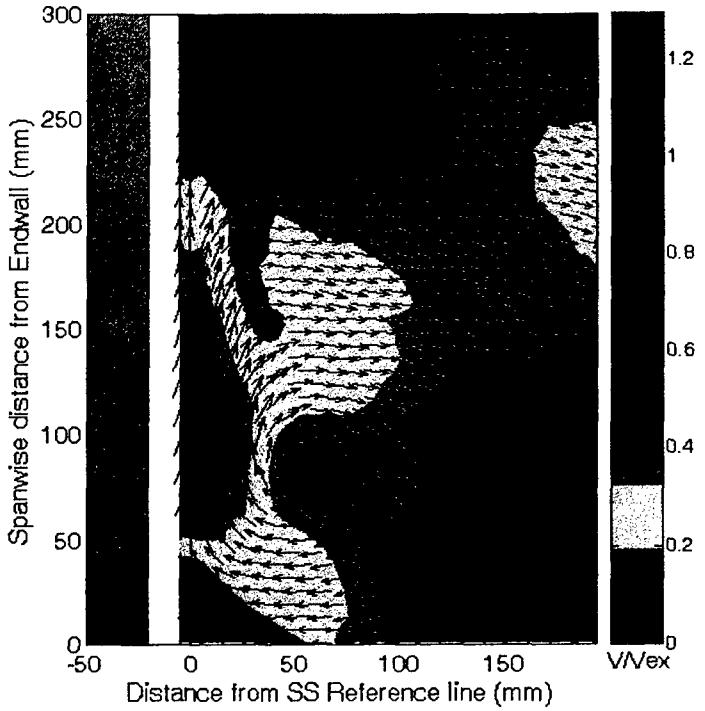

FIG. 7 Secondary flow at 63.5cm from TE for *t/h*=0%.

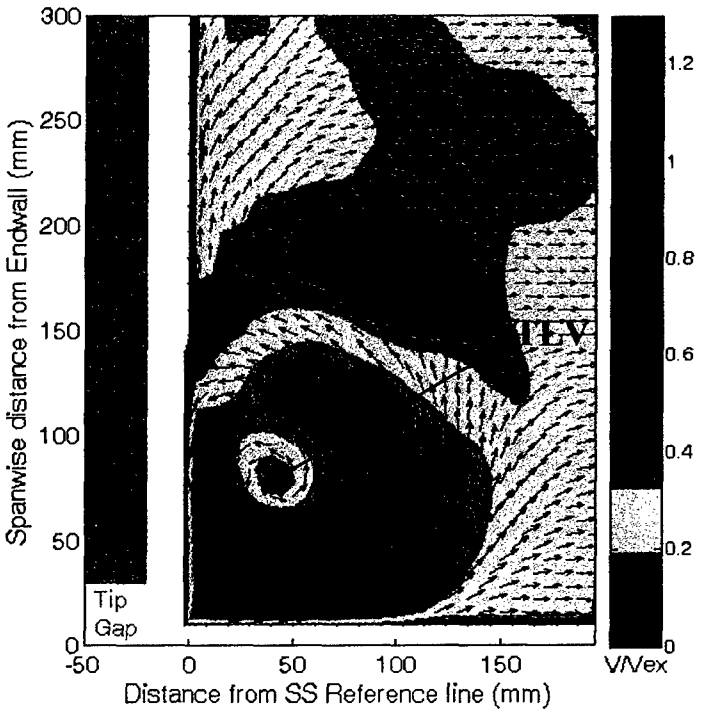

FIG. 8 Secondary flow at 63.5cm upstream from TE for *t/h*=1.68%, Moving Belt off.

Rather than extending further into the passage in the horizontal direction, the high magnitude flow extends further in the vertical direction. Since the TLV has been dragged closer towards the suction surface of the blade, the leakage jet that had become into the outer region of the vortex now continues vertically upwards and becomes part of the outer region of the PV. Similar to the results by Rao and Camci

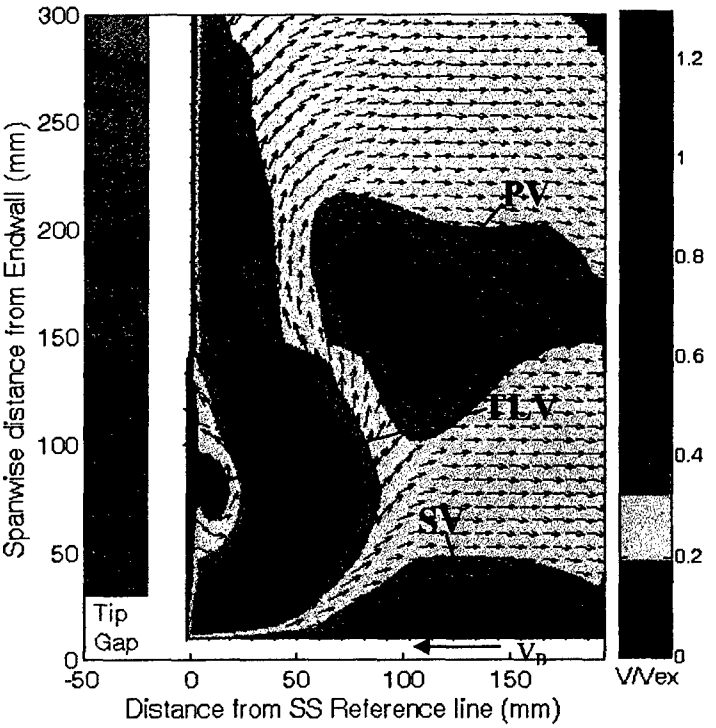

FIG. 9 Secondary flow at 63.5cm upstream from TE for *t/h*=1.68%, Moving Belt on.

[22] in a rotating rig, the PV was located above and slightly to the right of the TLV. Also, the tip leakage jet and opposing flow dragged by the moving belt generates a small vortex (SV) to the right of the TLV. This vortex has been observed in a rotating rig experiment by McCarter and Xiao [23] and was labeled the scraping vortex. In their study, they also measured the highest loses in the TLV.

Although not presented in this paper, measurements in the two planes further down stream, 43.5cm and 23.5 cm upstream from the TE, have been carried out. As the flow progresses further downstream, for both cases of endwall motion on and off, the TLV moves further away from the suction surface. For the case of no relative motion, the TLV progressively becomes more elliptical from the near circular shape seen at plane 63.5cm.

TIP FLOW NORMAL TO TIP SURFACE

The tip leakage flow was measured in planes vertical to the tip surface at three locations in the aft part of blade, in-line with the planes used for the secondary flow measurements. The behavior of the flow in the gap and its development into the tip leakage vortex may thus be seen. Figure 10 presents the measurements, with and without relative motion, at plane 63.5cm upstream from the TE for a gap of 1.68%Span. Measurements have also been taken at planes 43.5cm and 23.5cm from the TE, but due to space limitations are not presented in this paper. As in the case of the secondary flow measurements, small areas of the flow near the endwall and tip surface are not visible due laser reflections, but these are less than 3mm from the endwall and less than 1mm from the tip surface. Also, flow measurements

were not possible in the area above the tip gap adjacent to the pressure side and suction side of the blade, due to illumination or viewing difficulties. Unlike the secondary flow measurements, the velocity vectors are all of the same size and are overlapped with the scalar map of the velocity magnitudes. It was decided to use same-size vectors in order to be able see the smaller velocities in the separation bubble.

From the scalar maps presented in Figure 10, for the plane located at 63.5cm upstream from the TE, the acceleration of the leakage flow is clearly displayed. In both cases, the flow accelerates to a maximum velocity that is 20% stronger than the cascade exit velocity. For the no relative endwall motion case, the separation bubble is clearly defined and the flow appears to re-attach at around 65mm from the gap inlet. The presence of the endwall motion appears to reduce the height of the separation bubble by as much as half and reattachment seems to occur much closer to the gap inlet. Interestingly, the gap flow is not weakened by endwall surface moving in the opposite direction at this location in the blade. It can be seen that the effect of the moving endwall is to force its boundary layer under the leakage flow at the gap exit, pushing the high-speed leakage jet vertically. The development of this flow was seen earlier in the secondary flow measurements. The endwall boundary layer does not, however, have much effect on the flow in the gap, at this location in the blade.

It should not be assumed that the results presented in Figure 10 for that particular location in the blade are representative of the flow's behavior at other locations throughout the blade. At locations further downstream, the separation bubble was measured to be more similar in size for both cases of endwall motion on and off. In the planes further downstream, the flow was actually seen to be slightly strengthened by the opposing moving endwall. In locations very far downstream, where the blade thickness is smallest, the flow was seen not to reattach to the tip surface. Measurements were only carried out in locations in the aft part of the blade near the TE, but it is expected that the endwall motion has a more significant effect on the tip leakage flow at some locations in the upstream part of the blade where smaller velocities will be present.

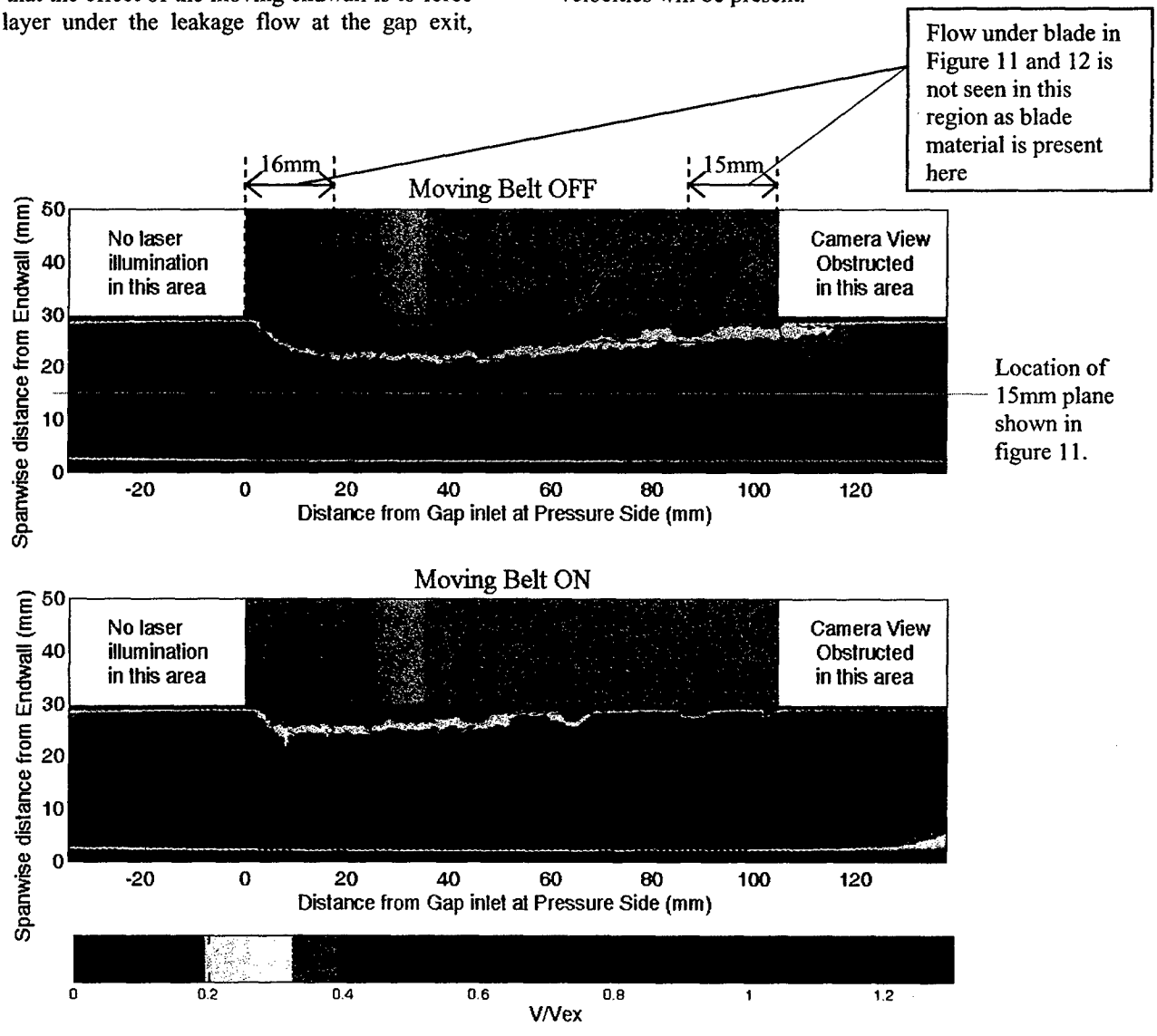

FIG. 10 Tip Leakage flow at 63.5cm from TE for t/h=1.68%.

TIP FLOW PARALLEL TO TIP SURFACE

Although the tip leakage flow measurements in the vertical planes have provided good insight on the behavior of the flow in the gap, the flow's behavior varies along the blade and it is important to have a complete picture of the entire flow in the gap. Although several studies have provided a great wealth of information concerning the flow in the tip gap, a complete 3-dimensional picture of the flow in the gap has never been presented. Although the ideal would be to achieve a volumetric flow field with 3-component vectors, the PIV technique used in this study only generates planar flow fields. However, by having a physically large gap and measuring planar flow fields at several locations within the tip gap, it has been possible to provide a more complete and detailed picture of the flow's behavior in the gap.

As stated previously, measurements were taken at several planes parallel to the tip surface within the 30mm gap. These planar flow fields within the tip gap are measured at regions T1, T2, T3 and T4 on the grid map (as shown in Figure 4). A portion of the flow field between T3 and T4 is missing due to camera view obstruction by pieces of the wooden spars of the blade located there. As was stated in the previous section, measurements were taken at planes in increments of 3mm for the range of 3mm to 27mm. However, for the purpose of clarity, the planar flow fields presented here are in increments of 6mm. As well, it should be noted that the original vector maps were processed to omit every certain pair of vectors in order to present vector maps that are not too crowded and can be clearly displayed. From Figure 4, it can be seen that the nose of the blade, which is not be confused with the leading edge, is located at 435mm in the axial direction. Measurements presented here are located between 485mm and 1100mm. Thus, the measurements are from 6.1% to 81.1% C_{ax}. Thus, the flow located in the last 20% C_{ax} of the blade is not captured. Likewise, the flow in the 6% C_{ax} from the leading edge is not captured. As stated previously, this is due to camera view obstructions and insufficient flow field area in narrow flow field regions under the blade, which produced weak correlations.

Figure 11 presents the flow field at the center of the gap (15mm from the endwall and tip surface). For the case of relative endwall motion on, an arrow has been drawn denoting the direction of the moving belt relative the blade, but it is not to scale. Looking first at the case for no relative endwall motion, the flow is seen to come into the gap at the LE at an angle close to that of the inlet flow angle and a progressive increase in velocity is seen in an axial direction up to about 30% C_{ax} of the blade. After 30% C_{ax}, regions of high velocity begin to appear very close to the pressure side of the blade and the flow takes a direction near-perpendicular to the blade camber-line. The high velocity regions near the pressure side of the blade vary along the blade depending on the blade loading. These high velocity regions near the pressure side remain present until about 75% C_{ax} in the blade.

In the case of relative motion on, the flow enters the gap at the leading edge at a slightly steeper angle than that of the inlet flow angle. Similar to the case with no endwall motion, a progressive increase in velocity is seen to occur in the axial direction. However, this increase occurs at a much slower rate than in the non-moving wall case and seems to carry through until much further downstream in the blade. As shown in the plot, the flow still crosses over from the pressure to the suction side of the blade in a near-perpendicular direction to the camber line, but the flow generally remains of the same magnitude as it crosses the gap. At about 60% C_{ax}, a region of higher velocity appears at the gap inlet on the pressure side. In fact, the flow in the aft part of the blade seems to be unaffected by the moving endwall and behaves very similar as in the case of no endwall motion. With the exception of the flow in the aft part of the blade near the trailing edge, a reduction in the magnitude of the velocities in the gap is observed.

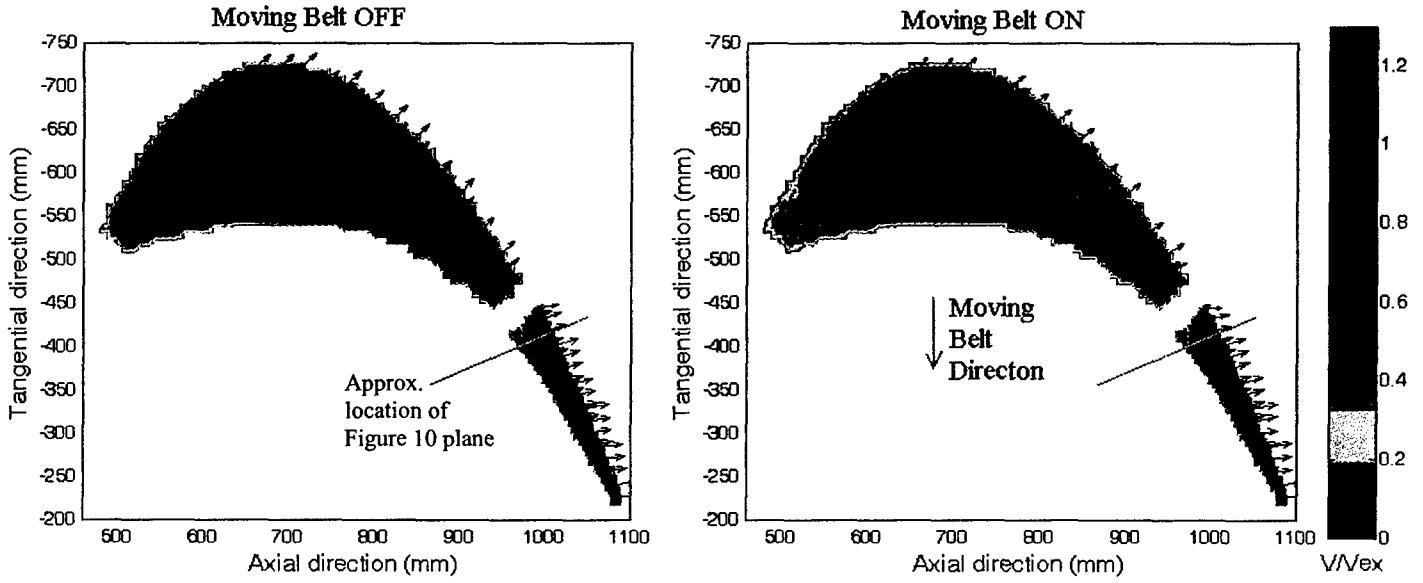

FIG. 11 Flow field in plane 15mm from the endwall for 30mm gap (t/h=1.68%). Note that the field of view does not extend to the outer blade surface (See Figure 4).

Stacked planar flow fields for a gap clearance of 1.68%Span are presented in Figure 12 for both cases, with and with out endwall motion. It an can be seen in both cases that the highest velocities are in fact found in the aft part of the blade, around 1000mm in the axial direction (65% C_{ax}). The flow separation at the gap inlet on the pressure side is clearly visible in both cases, as the flow closer to the tip surface tends to turn towards the pressure side of the blade. This is clearly visible at plane 27mm where some of the flow is completely directed towards the pressure side, which signifies the presence of the re-circulating flow. Measurements taken along the mean camber line by Yaras and Sjolander [8] also revealed a spanswise variation in the magnitude and direction of the velocities close to the tip. In their slender blade, the presence of the separation bubble was clearly evident after a quarter of the chord length from the LE. In Figure 11, the presence of separation bubble is seen to commence at about 18.5% C_{ax} from the LE for both cases of moving belt on and off.

In case of the relative endwall motion off, the flow at plane 27mm seems to be of very low velocity in the aft part of the blade, which is probably due to the velocity plane being measured in the core area of re-circulating flow in the separation bubble. In this area in the plane at 27mm, the flow seems to split off into two parts, the flow near the pressure side, which is directed towards the PS, and the flow near the suction side, which leaves via the SS. The latter is that part of the flow that has gone over the separation bubble and is trying to reattach as it exits the gap.

With relative endwall motion, the flow behaves differently at plane the 27mm from the endwall. The flow progressively changes direction and far down stream closer to the TE the flow is seen to be completely directed towards the pressure side of the blade. The presence of the moving endwall seems to change the flow within the separation bubble. The measuring plane at 27mm now lies in the top portion of the re-circulating flow. Obviously, some of the flow further upstream is not part of the separation bubble as it turns to exit from the SS.

A general reduction in magnitude of the gap flow due to the endwall motion is observed throughout most of the blade, except for the aft part near the trailing edge. Yaras and Sjolander [8] also reported a global reduction in velocity magnitude due to the relative endwall motion. As expected, the reduction is most apparent at the planes closest to the moving endwall. For example in plane 3mm, the vectors are clearly significantly smaller for most of the blade and the direction is more axial. The insignificant effect of the endwall motion on the flow in the aft part of the blade seen in these flow fields is clearly displayed in the tip flow measurement, previously presented in planes normal to tip surface, where these were carried out at a location in the aft part of the blade.

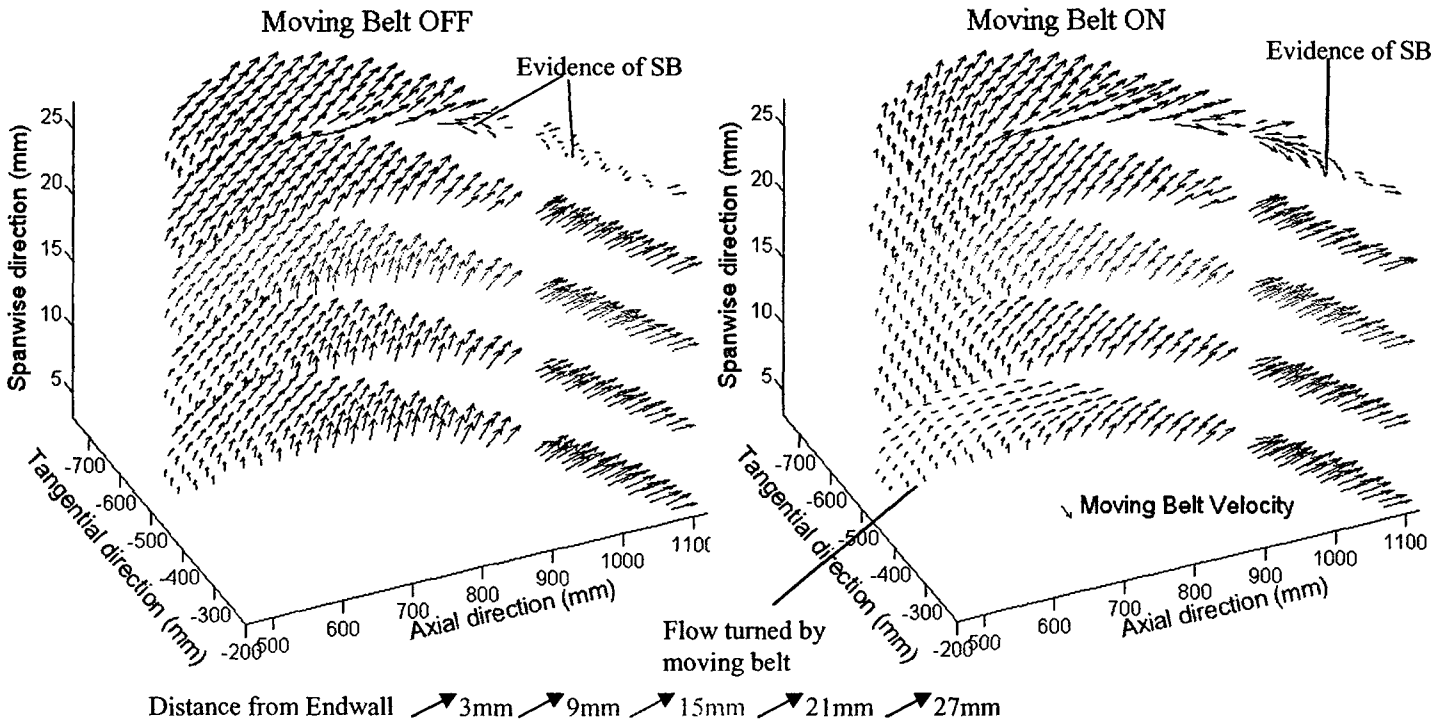

FIG. 12 Plots of 2-D flow fields in 3-D graphs for *t/h*=1.68%. At Figure 11 you can see the planes that are 15 mm from the endwall with magnitudes.

Flow Unsteadiness

It is well known that the flow in turbines can be unsteady. The results that have been presented above are those averaged over a period of 10 seconds, captured at 15 frames per second. Figure 13 displays four instantaneous

vector maps taken consecutively over a period of 0.20 seconds at 1/15th second time intervals.

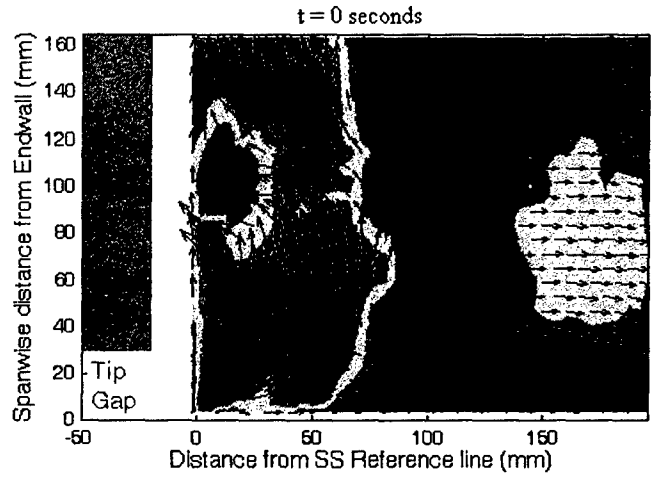

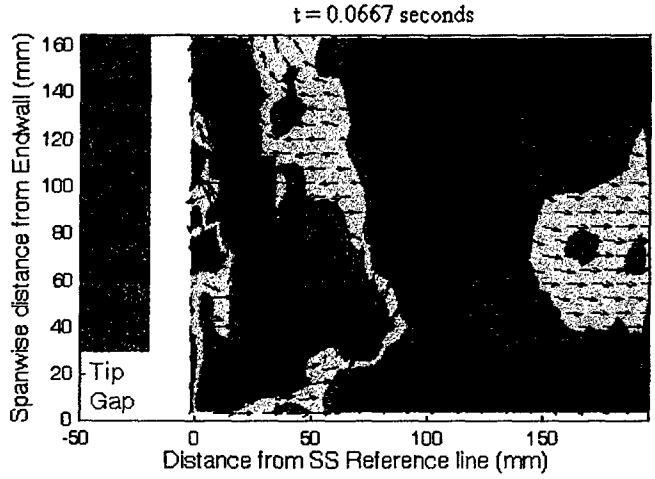

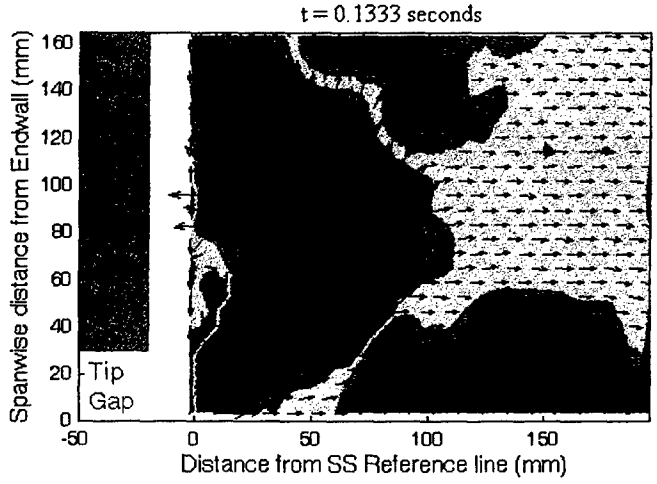

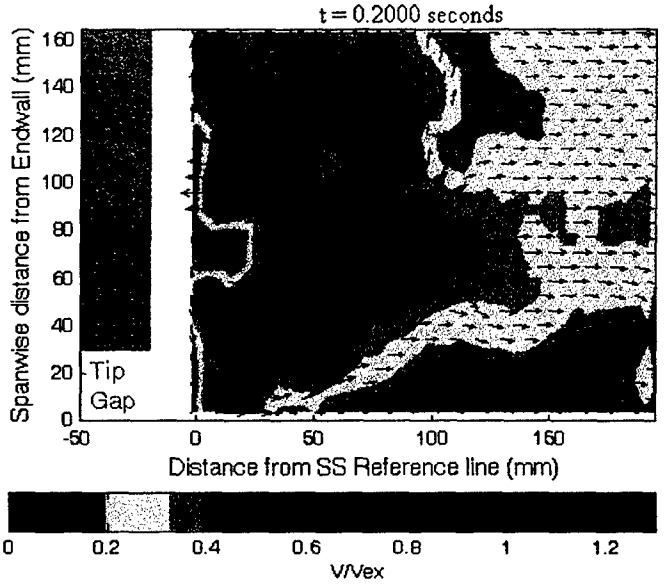

FIG. 13 Instantaneous vector maps at consecutive time intervals of lower part of secondary flow at 63.5cm from TE for t/h=1.68%, Moving Belt On. Averaged results over 10 seconds shown in Figure 9.

The flow shown is that of the lower part of the secondary flow (Figure 9) with a 30 mm gap and with the moving belt on. The flow is clearly unsteady, with the vortex core moving significantly. This unsteadiness is the subject of future study and the examples presented here might warn those researchers who are tempted to treat the averaged flows shown in Figures 7-12 as steady flows!

CONCLUSIONS

A very large-scale linear, 3-passage cascade has been developed to produce representative flow conditions around a central blade. This scale has enabled uniquely detailed PIV measurements of over-tip leakage flows and associated endwall flows in the blade passage to be made. This detail was possible due to the large tip gaps (up to 30 mm) employed. The relative motion between the turbine casing and rotor blade has been simulated with a moving belt.

The separation bubble under the tip has been clearly characterized, revealing its significant effect on the leakage flow. The moving endwall had a clear influence on the shape and size of the separation bubble. For example, at the plane examined the bubble was reduced to approximately half of its height from the case without endwall movement. This effect can be attributed to the shifting of the tip leakage vortex closer to the gap exit by the moving endwall, which pushes the exit jet upward and thus decreases the size of the separation bubble.

Dramatic influence of the tip flow on the passage vortex was observed in the secondary flow measurements. The passage vortex was weakened, distorted and relocated by the presence of the tip leakage vortex.

The relative blade–casing movement had a significant effect on both the tip leakage vortex and the passage vortex. The moving wall distorted the shape of the tip leakage vortex and moved both of the vortices closer to the suction surface.

The leakage jet and opposing moving belt generated a third vortex, labeled the scraping vortex in a previous study.

In the upstream portion of the blade there is a reduction in the magnitude of flow velocity in the gap. Further downstream, near the trailing edge, the velocities are largely unaffected by the blade-casing relative motion.

Although the flow studied here is known to be 3-dimensional, it has been investigated using a 2-dimensional PIV technique. Great insight to the behavior of the flow in and around the tip region has been provided, however these results are not complete as they lack a third velocity component. Thus, the results presented should be looked at as planar flow fields and not volumetric flow fields.

Further PIV and heat transfer studies for different gap heights and tip geometries, together with the unsteadiness of the over-tip flow field, are underway

ACKNOWLEDGMENTS

This work is supported by the Air Force Office of Scientific Research under Grant F49620-02-0027 with Thomas Beutner as the technical officer. Their support is greatly appreciated. The authors also wish to extend their gratitude to Mr. Trevor Godfrey for his useful suggestions and contributions to the design, assembly and manufacturing of the experimental setup.

REFERENCES

[1] Booth, T. C., Dodge, P. R., Hepworth, H. K., 1982. "Rotor-Tip Leakage: Part 1 – Basic Methodology," ASME Journal of Engineering for Power, Vol. 104, pp. 154-161.

[2] Hirsch, C., (Ed.) AGARD-AG-328, 1993. "Advanced Methods for Cascade Testing."

[3] Moore, J., Tilton, J. S., 1987. "Tip Leakage Flow in a Linear Turbine Cascade," ASME Paper 87-GT-222.

[4] Heyes, F. J. G., Hodson, H. P., 1991. "The Effect of Blade Tip Geometry on the Tip Leakage Flow in Axial Turbine Cascades," ASME Paper 91-GT-135.

[5] Bindon, J. P., 1987. "Pressure Distributions in the Tip Clearance Region of an Unshrouded Axial Turbine as Affecting the Problem of Tip Burnout," ASME Paper 87-GT-230.

[6] Bindon, J. P., 1989. "The Measurement and Formation of Tip Clearance Loss," Journal of Turbomachinery, Vol. 111, pp. 257-263.

[7] Yaras, M. I., Sjolander, S. A., 1992. "Prediction of Tip-Leakage Losses in Axial Turbines," Journal of Turbomachinery, Vol. 114, pp. 204-210.

[8] Yaras, M. I., Sjolander, S. A., 1991a. "Effects of Simulated Rotation on Tip Leakage in a Planar Cascade of Turbine Blades, Part I: Tip Gap Flow," ASME Paper 91-GT-127.

[9] Yaras, M. I., Sjolander, S. A., Kind, R. J., 1991b. "Effects of Simulated Rotation on Tip Leakage in a Planar Cascade of Turbine Blades, Part II: Downstream Flow Field and Blade Loading," ASME Paper 91-GT-128.

[10] Yamamoto, A., 1988. "Interaction Mechanisms Between Tip Leakage Flow and the Passage Vortex in a Linear Turbine Rotor Cascade," Journal of Turbomachinery, Vol. 110, pp. 329-338.

[11] Yamamoto, A., 1989. "Endwall Flow/ Loss Mechanisms in a Linear Turbine Cascade with Blade Tip Clearance," Journal of Turbomachinery, Vol. 111, pp. 264-274.

[12] Mayle, R. E., Metzger, D. E., 1982. "Heat Transfer at the Tip of an Unshrouded Turbine Blade," Proc., Seventh Int. Heat Transfer Conference, Vol. 3, pp. 87-92.

[13] Chyu, M. K., Moon, H. K. Moon, Metzger, D. E., 1989. "Heat Transfer in the Tip Region of Grooved Turbine Blades," ASME Journal of Turbomachinery, Vol. 111. pp. 131-138.

[14] Srinivasan, V., Goldstein, R. J., 2003. "Effect of Endwall Motion on Blade Tip Heat Transfer," ASME Journal of Turbomachinery, Vol. 125, pp. 267-273.

[15] Bunker, R. S., Bailey, J. C., Ameri, A. A, 2000. "Heat Transfer and Flow on the First-Stage Blade Tip of a Power Generation Gas Turbine: Part 1 – Experimental Results," ASME Journal of Turbomachinery, Vol. 122, pp. 263-271.

[16] Azad, G. S., Han, J. C., Teng, S., 2000. "Heat Transfer and Pressure Distributions on a Gas Turbine Blade Tip," ASME Paper 2000-GT-194.

[17] Chana, K. S., Jones, T. V., 2002. "An Investigation On Turbine Tip and Shroud Heat Transfer," ASME Paper GT-2002-30554.

[18] Thorpe, S. J., Yoshino, S., Ainsworth, R. W., Harvey, N. W., 2004. "An investigation of the heat transfer and static pressure on the over-tip casing wall of an axial turbine operating at engine representative flow conditions (I) Time-mean results," Int. Journal of Heat and Fluid Flow, Vol. 25, pp. 933-944.

[19] Thorpe, S. J., Yoshino, S., Ainsworth, R. W., Harvey, N. W., 2004. "An investigation of the heat transfer and static pressure on the over-tip casing wall of an axial turbine operating at engine representative flow conditions (II) Time-resolved results," Int. Journal of Heat and Fluid Flow, Vol. 25, pp. 945-960.

[20] Gregory-Smith, D. G., Cleak, J. G. E., 1992, "Secondary Flow Measurements in a Turbine Cascade with High Inlet Turbulence," ASME Journal of Turbomachinery, Vol. 114, pp.173-183.

[21] Keane, R. D. and Adrian, R. J., 1992. "Theory of Cross-correlation Analysis of PIV images," Appl. Sci. Res. 49, pp. 1-27.

[22] Rao, N. M., Cengiz, C., 2004, "Axial turbine Tip Desensitization by Injection from a Tip Trench, Part 1: Effect of Injection Mass Flow Rate," ASME Paper GT2004-53256.

[23] McCarter, A. A., Xiao, X., Lakshminarayana, B., 2000. "Tip Clearance Effects in a Turbine Rotor, Part II: Velocity Field and Flow Physics," ASME Paper 2000-GT-0477.

[24] Palafox, P., Oldfield, M.L.G., LaGraff, J.E., and Jones, T.V., 2005, "PIV Maps of Leakage and Secondary Flow Fields on a Low Speed Turbine Blade Cascade with Moving Endwall," ASME Paper GT2005-68189.

Proceedings of GT2006
ASME Turbo Expo 2006: Power for Land, Sea and Air
May 8-11, 2006, Barcelona, Spain

GT2006 - 90425

BLADE TIP HEAT TRANSFER AND AERODYNAMICS IN A LARGE SCALE TURBINE CASCADE WITH MOVING ENDWALL

P. Palafox
Dept. of Engineering Science,
University of Oxford

M. L. G. Oldfield
Dept. of Engineering Science,
University of Oxford

P. T. Ireland
Dept. of Engineering Science,
University of Oxford

T. V. Jones
Dept. of Engineering Science,
University of Oxford

J. E. LaGraff
L.C. Smith College of
Engineering and Computer Sci.,
Syracuse University

ABSTRACT

High resolution Nusselt number (*Nu*) distributions were measured on the blade tip surface of a large, 1.0 meter-chord, low-speed cascade representative of a high-pressure turbine. Data was obtained at a Reynolds number of 4.0×10^5 based on exit velocity and blade axial chord. Tip clearance levels ranged from 0.56% to 1.68% design span or equally from 1% to 3% of blade chord. An infrared camera, looking through the hollow blade, made detailed temperature measurements on a constant heat flux tip surface. The relative motion between the endwall and the blade tip was simulated by a moving belt. The moving belt endwall significantly shifts the region of high Nusselt number distribution and reduces the overall averaged Nusselt number on the tip surface by up to 13.3%. The addition of a suction side squealer tip significantly reduced local tip heat transfer and resulted in a 32% reduction in averaged Nusselt number. Analysis of pressure measurements on the blade airfoil surface and tip surface along with PIV velocity flow fields in the gap give an understanding of the heat transfer mechanism.

INTRODUCTION

In unshrouded axial flow turbines, the unavoidable clearance between the rotating blade tips and the surrounding stationary casing is the cause of significant efficiency and heat transfer penalties. This gap allows passage fluid to flow from the pressure to the suction side of the blades, driven by the pressure difference across the blade. This tip leakage flow is accelerated through the gap reducing the work done on the blade, generating losses in the gap and eventually exiting on the suction side where it mixes with on-coming passage flow as it rolls up into the tip leakage vortex. An estimated 1-2% loss in turbine efficiency has been associated with a tip gap of 1% span [25]. Highly-loaded turbine rotors are especially affected by this leakage flow, where in addition to efficiency losses, elevated heat transfer rates in the vicinity of the tip can lead to the reduction of blade life. Tip heat transfer has recently become increasingly important as the turbine inlet temperatures are continuously being pushed higher in order to achieve high thermal efficiency and power output. The casing has also been found to become more affected by these heat transfer loads over the blade tip. Over the past couple of decades, several studies have contributed to the general understanding of the phenomena taking place in turbines. Linear cascades have been used extensively and have been successful in providing a better understanding of the physics involved [26]. While matching the blade loading, Reynolds number and other key parameters, linear cascades have simplified the problem and allow larger scale cascades providing greater detailed measurements in the tip region. The relative motion between the blades and the casing endwall is probably the most significant effect not simulated in most cascade experiments.

Early studies by Moore and Tilton [27] showed the acceleration of the flow into the tip gap and the formation of a vena contracta on the tip surface next to the pressure side. The flow subsequently experienced significant diffusion and mixing prior to exiting the gap on the suction side. In contrast to Moore and Tilton's model, where the tip leakage flow mixed fully prior to exiting the gap, Heyes and Hodson [28] proposed a model comprising an isentropic jet and a separation bubble wake, which took into account the effect of mixing in their thin-blade cascades. Increasing the amount of total mixing inside the tip gap increased the discharge coefficient. Also, the effect of boundary layer growth over the blade tip revealed a reduction of 5% in the discharge coefficient, thereby reducing the overall leakage loss. Using micro-tapping technique, Bindon [29] studied in more detail the pressure distribution in the tip region as affected by the tip gap height. He noticed a very low pressure coefficient on the suction side of his blade, an affect which reduced as the clearance gap was increased. He found the lowest pressure,

2.8 times smaller than cascade outlet pressure, occurred on the pressure corner. He also found the lowest pressures to occur at 60% chord and the pressures on the tip and endwall surfaces to increase with increasing tip gap height. In another study, Bindon [30] quantified for the first time the contributions by mixing (48%), internal gap shear (39%) and endwall/secondary flow (13%) to the overall tip clearance loss for a 2.5% C tip clearance gap. Yaras and Sjolander [31], using more slender blades with lower turning angle and higher gap clearance, found that a much lower loss was generated in the gap.

Yaras et al. [32] & [33] also studied the effects of the endwall relative motion on tip gap flow, downstream flow field and blade loading by employing a motor-driven belt with a thin-blade, low turning angle cascade. For a gap clearance of 3.8% C and Re=1.4 x 10^5, they found that although the shearing affect of the moving wall on the gap flow was quite small, it led to a decrease in the pressure difference across the gap and thus a reduction in the acceleration of the tip flow. The moving wall strengthened and drew the passage vortex towards the gap flow outlet (suction side) creating a throttling affect on the gap flow, which resulted in a 50% reduction of the mass flow rate through the gap. Measurements of the flow field, taken downstream of the TE, revealed enhancement of the passage vortex and weakening of the leakage vortex with increasing belt speed. A reduction in blade loading due to the moving wall effect was only noticeable at locations very near the tip.

Palafox et al. [34] recently presented detailed flow field maps of the leakage and neighboring secondary flow for measurements taken in a large scale cascade with a moving endwall. The geometry was that of a high turning angle blade, representative of a high pressure turbine, and the data presented was for a gap height of 1.68% span or 3% chord. The moving endwall was shown to push the tip leakage vortex closer to the gap exit and push the leakage jet upward away from the endwall along the blade suction side, also affecting the passage vortex and creating a scraping vortex. Detailed velocity maps of planes perpendicular to the tip surface showed the separation bubble clearly, revealing its effect on the leakage flow. The moving endwall was seen to reduce the size of the separation bubble by more than 50% at the plane measured. Time-resolved measurements revealed a flow with significant unsteadiness.

Yamamoto [35] looked at the interaction of the leakage flow with the passage vortex at a plane 24% C_{ax} downstream. He observed an insignificant interaction between the two vortices for a low tip clearance of t/b=1.3%, but noticed stronger interaction with increasing clearance. The stronger leakage vortex pushed the passage vortex, which became weaker, towards the pressure side of the passage. In a later paper [36], detailed velocity vectors and streaklines on a blade-to-blade plane between the endwall and tip surface as well as total pressure contours on a downstream plane were presented. These effectively showed the relationship between the tip leakage and endwall flow and cascade loss generation.

In an early heat transfer study, Mayle and Metzger [37] looked at the effect of the relative blade-casing motion on the tip heat transfer using a simple rectangular profiled stationary model with concave surface adjacent to a motor-driven, rotating disk. The effect on the heat transfer due to the relative motion was found to be negligible over a range of parameters tested. In a later study, Chyu et al. [38] also found that the relative motion had negligible effect for their simple grooved tip model. In a more recent study by Srinivasan and Goldstein [39], the heat transfer on the tip was studied in a linear cascade incorporating a moving wall apparatus with the use of naphthalene sublimation technique. Very little effect of the moving wall was found in the region near the trailing edge. However a 9% reduction on the heat transfer was found to occur at mid-chord locations for a gap of t/C=0.6%. It was speculated that the tip leakage vortex moving closer to the suction surface was the cause of this reduction. Interestingly, an increase in their measured Sherwood number was found in some regions in the upstream half of the blade. A slight increase was also found in the region near the TE for a gap of t/C=0.86% with the introduction of the moving wall. No effect due to relative motion was seen at larger clearance gaps. Other tip heat transfer studies where no relative motion has been simulated includes that of Bunker et al. [40] and Azad et al. [41] where detailed heat transfer coefficient maps on the tip surface have been provided for a range of tip clearances and two turbulence intensities. Increases in the overall heat transfer were found in both cases for increasing gap clearances and increasing turbulence intensities.

Some recent studies have also focused on studying the effect of the tip flow on the heat transfer of the adjoining casing wall. Chana and Jones [42] used thin film gauges to measure the heat transfer on the casing wall and flow adiabatic wall temperature in the gap of their QinetiQ Isentropic Light Piston Facility (ILPF) with correct non-dimensional engine conditions. The casing was shown to suffer the highest heat transfer as the rotor blades pass under it; the high heat transfer rates were attributed to the tip leakage flow. In a 2-part paper presented by Thorpe et al. [43] & [44] , detailed heat transfer and pressure measurements were provided for the over-tip casing wall of their Isentropic Light Piston Tunnel, which operates at engine representative conditions. These confirmed the general results of Chana and Jones [42] that the casing heat transfer peaks as the tip passes the casing. Given the previous research studies, there is still a need for the further aerodynamic studies, with higher spatial resolution, in order to better understand the behavior of the flow in tip region and how this flow is related to the heat transfer. These studies are especially important in cascades that are representative of high-pressure turbines with relative motion simulation, where data is very scarce or non-existent.

In the present paper, the recent Oxford research work using a large-scale linear cascade with a moving belt is introduced. Particle Image Velocimetry, PIV, is used to provide detailed measurements in the restricted region of the tip gap. Detailed results are presented for the gap region and adjacent passage flow for the largest gap clearance studied.

NOMENCLATURE

A_S	Surface Area
AC	Alternating current
b	Blade span
C	Blade chord
C_{ax}	Blade axial chord
CCD	Charge-coupled device
C_P	Static pressure Coefficient = $\frac{P_{01} - P_S}{P_{01} - P_{S2}}$
DC	Direct Current
e	Emissivity
H	Shape factor
h	Heat transfer coefficient
IR	Infra-red
k_f	Thermal conductivity of the fluid
LE	Leading edge
L	Tip gap length or thickness; Characteristic length
L_{max}	Maximum blade thickness
MOFF	Relative Endwall Motion OFF
MON	Relative Endwall Motion ON
$\dot{m}$	Mass flow rate
Nu	Nusselt number
P	Static pressure
P_0	Total pressure
PIV	Particle image velocimetry
Pr	Prandtl number
PS	Pressure side surface of blade
q	Dynamic pressure
$\dot{Q}$	Heat rate
R	Reattachment location
Re	Reynolds number
SB	Separation Bubble
s	Blade pitch
SS	Suction side surface of blade
SSS	Suction-Side Squealer
St	Stanton number
T	Temperature
t	Gap height
TE	Trailing edge
Tu	Turbulence intensity
TET	Turbine inlet temperature, turbine entry temperature
V	Velocity, Voltage
V_{ex}	Cascade exit velocity
V_B	Belt velocity
δ	99% boundary layer thickness
δ^*	Displacement thickness
θ	Momentum thickness

Subscripts

s	Static conditions, surface measurement
g	gas conditions
0	Total conditions
1	Cascade inlet conditions
2	Cascade outlet conditions
4	Upstream conditions

EXPERIMENTAL APPARATUS AND PROCEDURES

TEST CASCADE AND TEST SECTION

In order to study of the tip leakage flow in great detail, the geometry of the cascade design used in this investigation was scaled up to a blade chord length of 1 meter. In doing so, it allows for measurements to be conducted in tip clearance gaps of up to 30 mm height, which is equivalent to a 1.68% span or 3% chord. Fig. 2 and 1 summarize the cascade geometry and test conditions used in the present study. As illustrated in the figure, the cascade arrangement was set up inside an existing 2 m × 4 m suction type wind tunnel [45]. In order to achieve the design turning angle, part of the wind-tunnel's left wall was removed and a new bell-mouthed inlet, which provides the inlet flow to the cascade, was set up there. The previously existing inlet to the wind tunnel was blocked off.

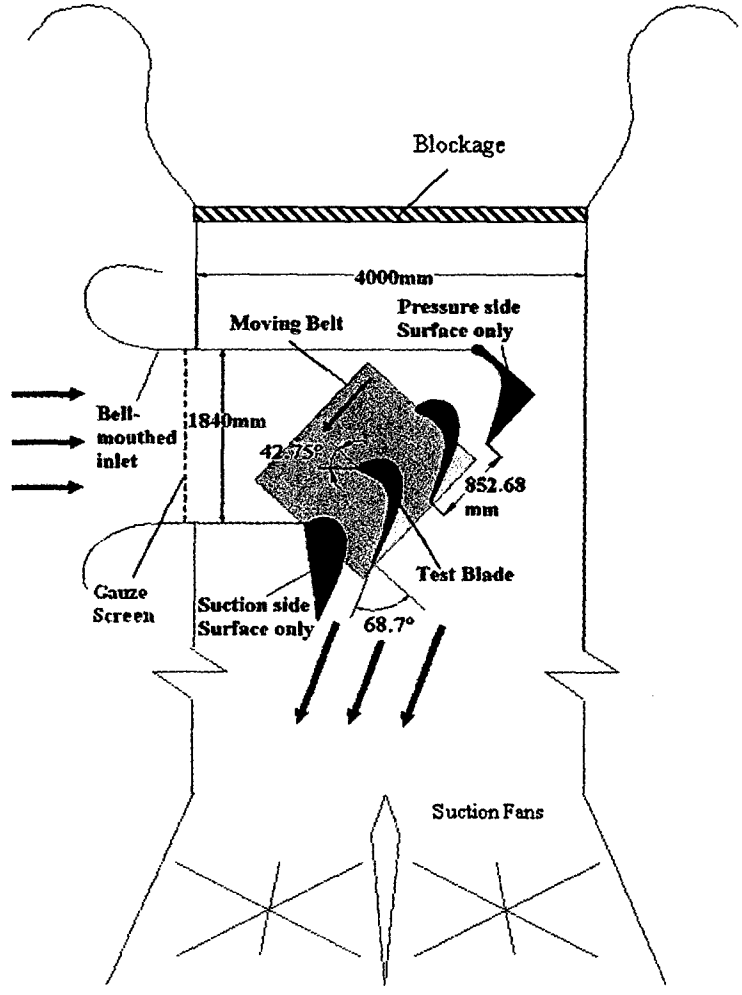

Fig. 1 Cascade Geometry and Test Conditions. The cascade was mounted in an existing large wind tunnel.

Table 2 Blade Properties and Flow Conditions

Blade Chord, C (mm)	1000
Blade Axial Chord, C_{ax} (mm)	808
Blade maximum thickness, L_{max} (mm)	243
Blade Pitch, s (mm)	853
Design Span, b (mm)	1785.6
Actual Span (mm)	1000
Inlet Flow angle (degrees)	42.75
Blade Exit angle (degrees)	68.7
Reynolds No. (based on V_{ex} and C_{ax})	4.0×10^5

The blade profile and cascade geometry used was an ERCOFTAC test case comprehensively tested at Durham University by Gregory-Smith [46] for research mainly in secondary flow without tip gap. The profile of the blade is that of a high-pressure turbine with a high turning angle of 111.45°. It should be noted that actual blade span was chosen to be nearly half of the design span after smoke visualization tests revealed no interaction between the hub endwall and the tip endwall secondary flows at a 1 meter span. Two fully-profiled and two semi-profiled blade models were used in a three-passage linear cascade. Passage flow measurements were conducted in the centre passage and tip-leakage flow measurements were conducted on the blade labeled "test blade". The blades were made from flexible plywood, which were wrapped around profiled ribs. The test blade differs from the other models in that it is mostly hollow throughout, which is an important part of the design, as will be seen in later sections, when measuring the tip flow without any interference.

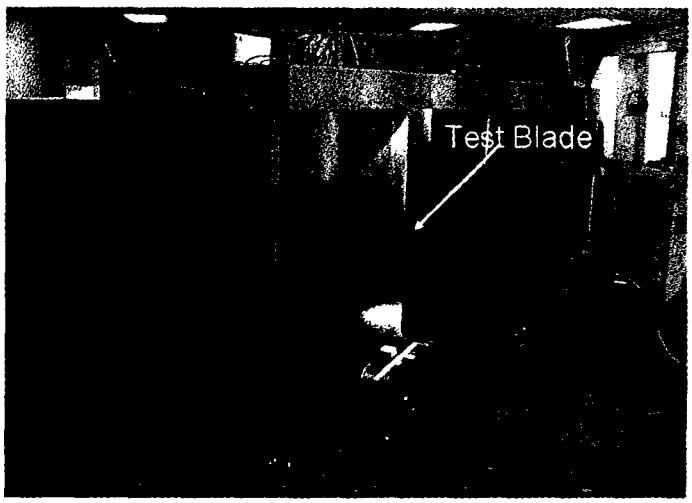

Fig. 2 Cascade test section and moving belt.

The arrangement of the cascade inside the 2 m × 4 m wind tunnel, used to generate the appropriate conditions, is illustrated in Fig. 2. As shown, the blade models were secured to a frame, which was fixed to the tunnel floor. Under the suspended blades sits a motor-driven belt system. The moving belt system and wooden boards that make up the endwall were set up on individual frames with height-adjusting feet to allow for the changing of the tip gap clearance.

The moving belt, designed to simulate the relative motion between the rotor blades and casing wall, completely covers the area under the test blade and center passage where measurements are taken. The belt extends over half an axial chord length upstream of the leading edge of the blade in order to produce a representative skewed inlet boundary layer in tests simulating the relative motion. The belt was made of a top layer of polyurethane (facing the flow) and a lower layer of polyester with a total thickness of 2 mm. The belt sits on a perforated plate, which is the cover of a vacuum box, and is tensioned by a pair of aluminum rollers at the ends. A 7.5 kW AC motor with a variable speed controller drives one of the rollers, which drives the belt across the cascade at a constant velocity. Vertical displacements of the belt have been measured to be less than +/- 0.05 mm with suitably adjusted tensioning and suction applied by the vacuum box. The belt desired belt speed is calculated from the blade velocity triangles and is set at 1.34 times the inlet velocity. The belt system is sealed off in the front part with tape and the gaps at the sides are kept to a minimum and far away from the flow of interest.

Upstream Boundary layer properties and turbulence intensity values are summarized in Table 3. The measured pressure profile on test blade was compared with results of Durham University and revealed excellent match, assuring the correct driving pressures are present for adequate leakage flow behavior. Periodicity was not investigated as the main interest lied in the tip leakage flow, which was confirmed by the correct pressure distribution around the blade. Comparison of blade pressure distribution with Durham University's results and other useful information can be found in [34]. The effect of turbulence intensity is not investigated here but this paper will serve as a baseline for future investigations into varying turbulence intensity and other parameters.

Three tip gaps heights of 10 mm, 15 mm and 30 mm, equivalent to 0.56%, 0.84% and 1.68% design span (1785.6 mm) or 1%, 1.5% and 3% chord, respectively, were tested for the flat tip case. A suction-side squealer tip geometry with a 15 mm gap is also investigated. The depth of the suction side squealer is 15 mm with a thickness of 5 mm. The suction side squealer extends from the end of the leading edge arc up to the beginning of the trailing arc on the suction side, shown in black in Fig. 3. The suction side squealer is rounded at the leading edge to avoid separation of the flow.

This paper presents the heat transfer, pressure and velocity measurements for all the tip gap heights studied with and without relative endwall motion.

VELOCITY MEASUREMENTS WITH PIV

Particle Image Velocimetry, PIV, has been used to measure the flow inside and around the gap region, including the adjacent secondary flow, with and without tip gap. Description of the PIV equipment and measurement setup for different survey planes and regions is described in [34]. The PIV data presented in this paper is that of the mid-gap flow on planes parallel to the gap surface, taken from [34] for the purpose of comparison with tip pressure data, and of gap measurements in planes perpendicular to the tip surface, one taken from previous paper for comparison and 2 new measurement sets.

Fig. 3 shows the location of the perpendicular flow measurement planes over the true blade material profile. As shown, the planes are referenced to the trailing edge and are perpendicular to the Suction Surface Reference Line, which aligns with the latter straight part of the blade surface near the trailing edge. All data sets are presented with the blade surface profile shown, together with the internal blade-model profile showing the actual area of the measurement window.

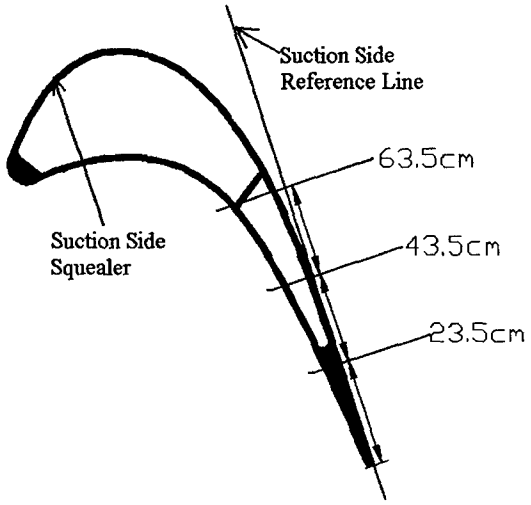

Fig. 3 Location of Measurement Planes Perpendicular to tip surface inside Gap.

Particle Image Velocimetry, PIV, [34] measures fluid flow fields by tracking the movement of particles seeded into the fluid. For each test, a total 150 pairs of instantaneous vector maps were generated and these 10 seconds worth of data were averaged to give the mean flow results presented in this paper. Instantaneous, unsteady flow results will be presented in a future paper.

PRESSURE MEASUREMENTS

Static pressure measurements were taken on the blade profile surface and on the tip surface for the various conditions. A *Scanivalve* system was employed that allows for a total of 48 pressure measurements to be taken in a single test, scanning through sequentially with the use of a single piezoresistive transducer. Pressure measurements were taken over a period of 3 seconds per reading.

The blade airfoil surface pressure measurements were taken at a 10% chord distance from the blade tip. A total of 44 pressure tappings were placed on the blade profile. Tip surface pressure measurements were taken at 9 equally-spaced axial locations with 4 equally-spaced locations in the tangential direction, for a total of 36 measurements. The results were interpolated in a *Matlab* code and are presented with the location of the measurements indicated.

HEAT TRANSFER MEASUREMENTS WITH IR CAMERA

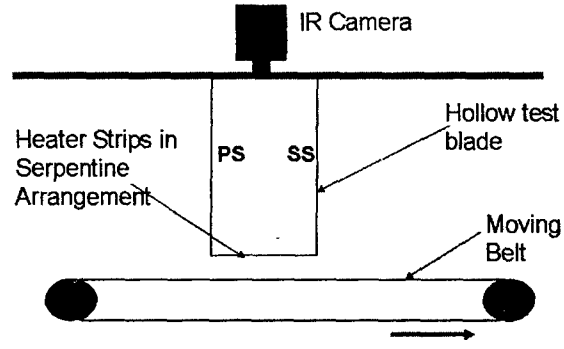

Fig. 4 Heat Transfer Experiment Setup.

Blade tip heat transfer measurements were carried out with the use of an infra-red camera. The IR camera, fixed to the supporting Perspex to that which the test blade is fixed, looks through the hollow blade onto the internal surface of the blade tip (Fig. 4). The blade tip is replaced by a thin, constant heat flux electrical heater design. The tip flow generates a temperature distribution on the tip surface during each test run. The IR camera measures surface temperatures on the inside surface of the heater at high spatial resolution over the large tip surface area. A total of 40 measurements are taken per data set at a frequency of 5 Hz; thus 8-seconds averaged measurements are used. The heat transfer coefficients can be calculated by also measuring the free-stream temperature and heat rate, as shown by Equation 1.

$$h = \frac{\dot{Q}}{A_S (T_S - T_g)} \qquad (1)$$

A new design of copper heater strips in a serpentine arrangement, shown in Fig. 5 was used for generating the constant heat flux on the blade tip surface. In the enlarged CAD drawing of the leading edge part of the heater tip, it can be seen that the rectangular copper strips are connected in series covering the entire measuring window. Sheet of 18 microns thick Copper and 42 microns thick Kapton were photo etched into series of 5 mm wide rectangular strips with 0.5 mm gaps between neighboring strips that take the shape of the blade at the outer edges. A hollow Aluminum rim, of thinner walls than that of the blade material, is glued onto the blade. A profiled sheet of Upilex of 50 microns in thickness is glued to the profiled rim with glue, also 50 micron-thick, and

covers the entire blade tip. The individual sheets of copper strips with Katpon backing are glued onto the profiled Upilex sheet covering the entire blade, making the total thickness, from inner tip surface to outer tip surface, of the tip 210 microns (Fig. 6). The total area covered with copper is 0.1452 m^2. The copper strips cover most of the blade tip surface with the exception of a small part near the trailing edge.

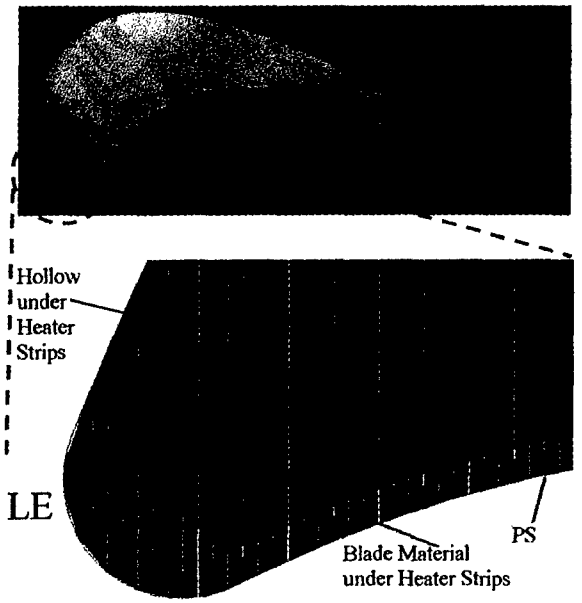

Fig. 5 Copper Heater Strips Serpentine Design.

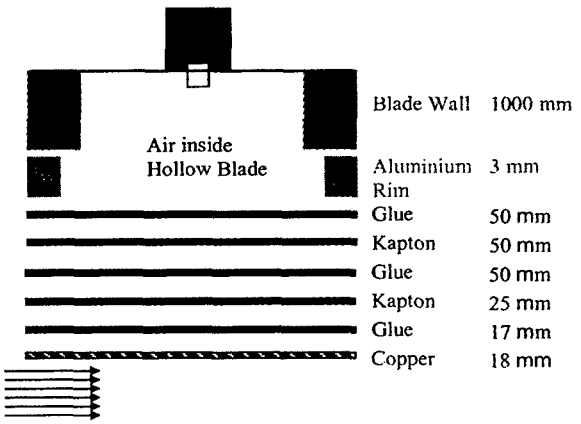

Fig. 6 Layers of material comprising blade tip.

The strip at the leading edge and the strip closest to the trailing edge are soldered to wire leads which connect to a DC power supply. The voltage drop across the heater strips are measured along with the current in each test run. The free stream temperature is measured with a thermocouple 1-meter chord upstream of the leading edge. Emissivity values for the copper and tip inner surface, painted matt black, were previously calibrated with the IR camera. Thus, Equation 2 is used to extract h values from the temperature measurements on the tip surface taken with the IR camera. The temperature of the surroundings, mainly that of the moving belt surface, was taken to be the gas temperature in the equation below. Experiments were conducted with a sealed tip and losses due to free convection inside the blade were measured and are accounted for in the computation of h. Some lateral conduction exists very near the edges of the measurement maps. Conduction through the blade tip material was computed and found to give an insignificant temperature drop across the tip.

$$h = \frac{\frac{V \cdot I}{A_S} - \varepsilon\sigma(T_S{}^4 - T_g{}^4)}{T_S - T_g} \qquad (2)$$

Results are presented in terms of Nusselt number based on axial chord length and free stream thermal conductivity.

EXPERIMENTAL RESULTS AND DISCUSSION

Velocity Fields in Tip Gap

PIV Maps of the flow in the mid-gap plane for the 1.68% span case are presented in Fig. 7 and Fig. 8, with and without moving endwall, respectively, with blade profile delineation for mapping data. These results are compared with the new data presented in this paper and aid in the understanding of the tip flow.

All PIV results are presented with the same color scale that allows clear distinction of the overlaid vectors.

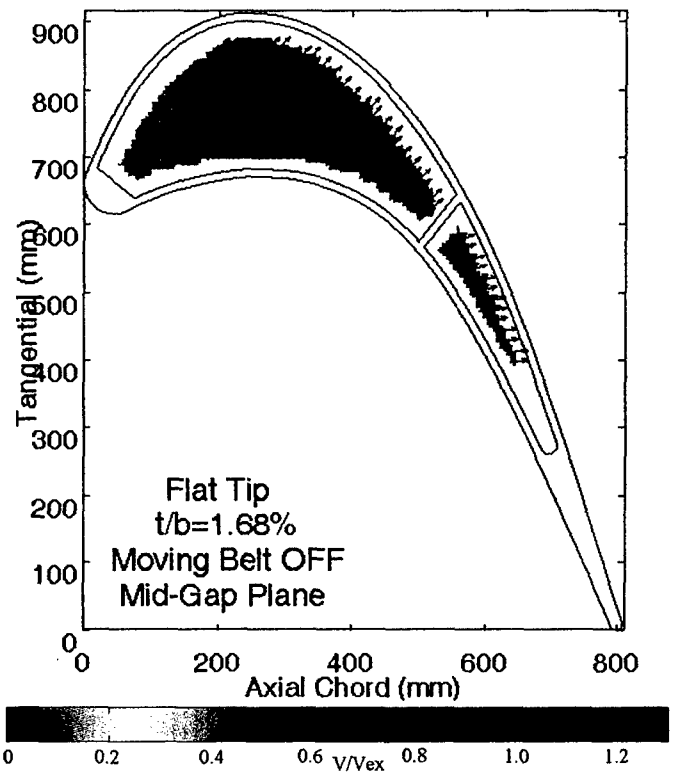

Fig. 7 PIV Flow Field for t/b=1.68% with No Relative Motion (previously presented in [34]).

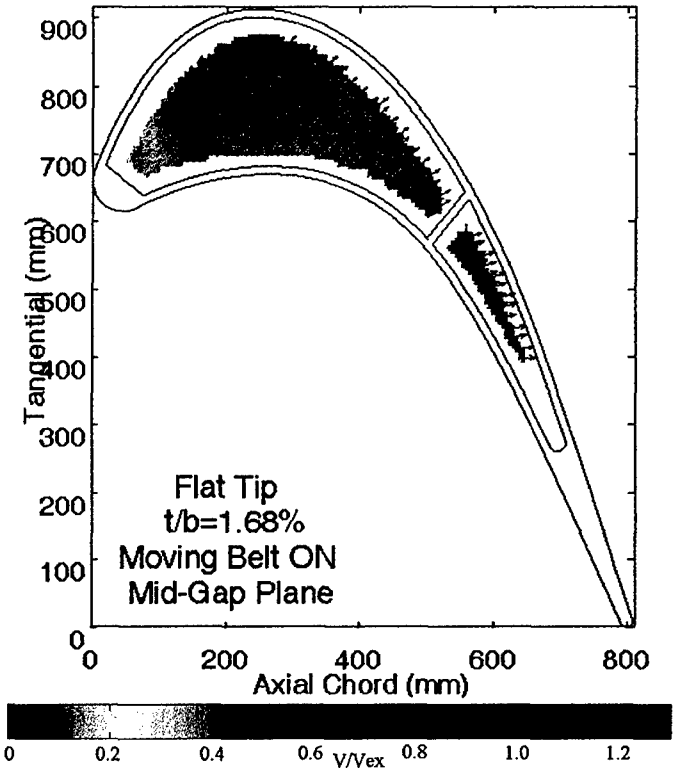

Fig. 8 PIV Flow Field for *t/b*=1.68% with Relative Motion (previously presented in [34]).

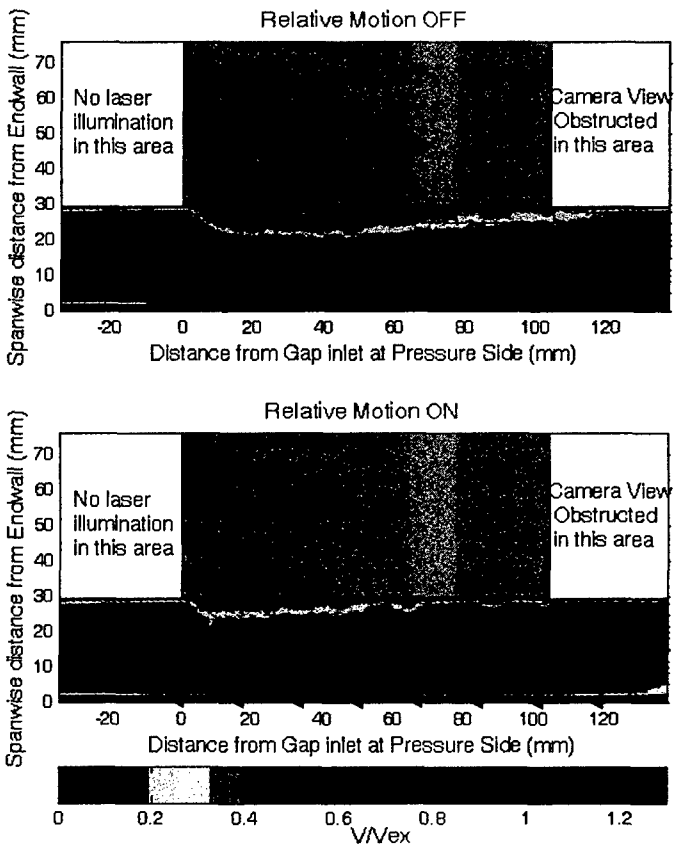

Fig. 9 Perpendicular leakage flow at 63.5cm from TE for *t/b*=1.68% (previously presented in [34]).

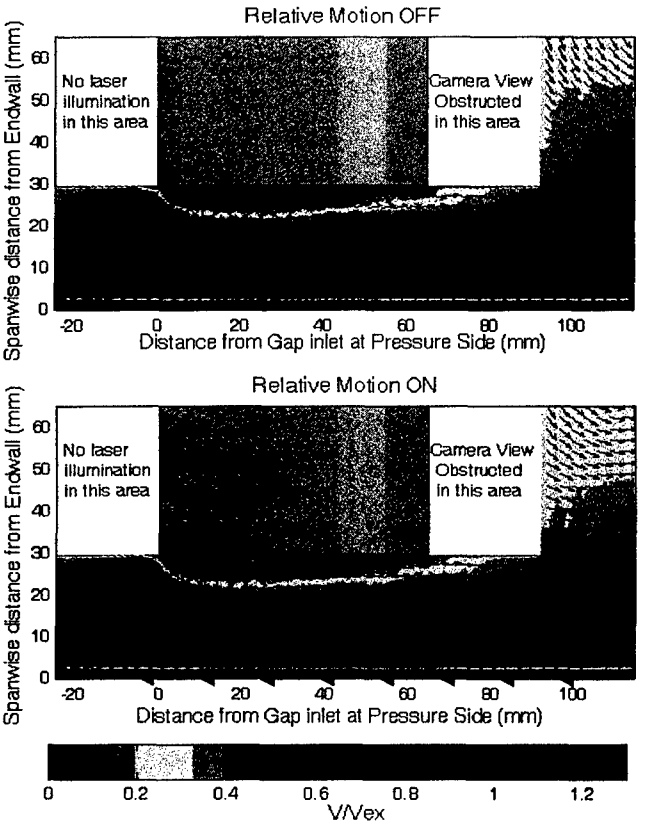

Fig. 10 Perpendicular leakage flow at 43.5cm from TE for *t/b*=1.68%.

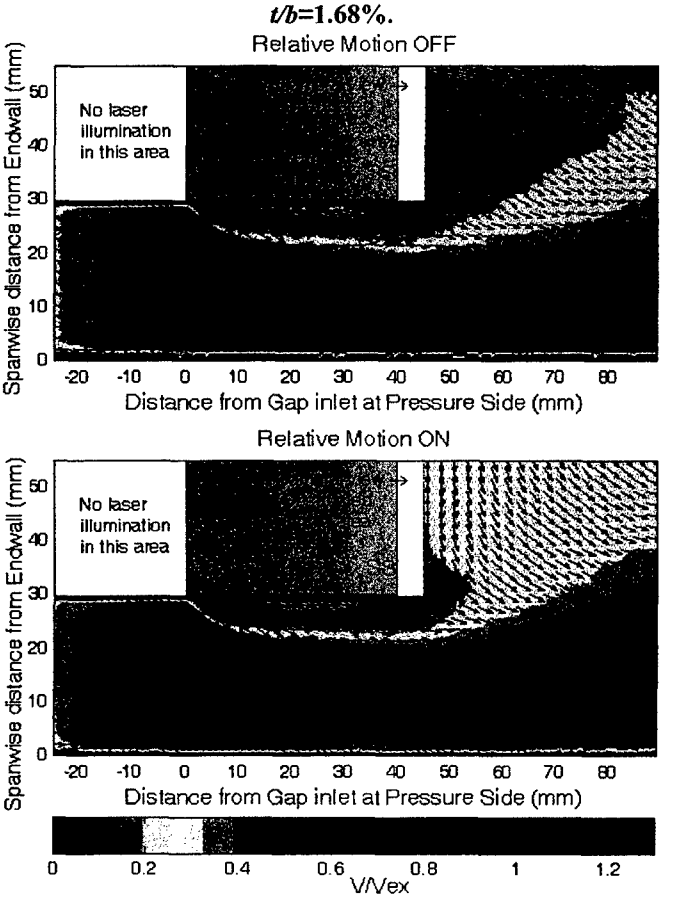

Fig. 11 Perpendicular leakage flow at 23.5cm from TE for *t/b*=1.68%.

Velocity maps for perpendicular planes in the gap are presented for the three locations shown in Fig. 3 for the flat tip with 1.68% *b* gap. In Fig. 9 it can be seen how the flow is accelerated through the gap forming a separation bubble, which is reduced significantly by the moving endwall at this location. Moving to the plane 43.5 cm from the TE (Fig. 10), the flow is shown to reattach for both cases of moving and stationary endwall, but the separation bubble is less affected by the moving endwall case at this location. Interestingly, the flow for the moving endwall case experiences higher velocities at this location than the stationary endwall. Reattachment seems to occur at similar locations for both cases of moving and stationary endwall. At the plane of measurement closest to the TE (Fig. 11), the flow is clearly seen to separate and not reattach on the tip surface for both endwall motion cases. The velocities are significantly lower than for those measured in the planes further upstream.

These velocity results will be referred to later in the paper in relation to the heat transfer measurements.

Pressures on Blade Tip

Tip pressure measurements on the blade tip for the cases investigated are presented in terms of pressure coefficient, C_P, defined by upstream total and downstream static pressures. The star symbols overlapping the pressure coefficient distributions denote the locations where the pressures were measured. In the following discussion it is assumed that a high pressure coefficient infers a high velocity and vice versa. Looking at the pressure plots for the 1.68% *b* gap height in Fig. 12, the flow is seen to increase in velocity in the axial direction for the front part of the blade. For the case with stationary endwall, the velocity gradients in the direction across the tip are noticeable at around 40% C_{ax}. The region of highest velocity is seen around 60 to 70% C_{ax}. In the case of moving endwall for the same clearance, the velocities at the front part of the blade are seen to be lower than those for the case with stationary endwall. Also, the cross-tip velocity gradients become noticeable at around 60% C_{ax}, significantly further downstream. The region of highest C_p is seen to be around 70% C_{ax}. These results agree well with the velocity measurements taken at the mid-gap plane for the same conditions and the results for the perpendicular planes in the tip gap. The reader should be aware that the PIV results shown in Fig. 7 and Fig. 8 cover more area than the pressure results in some parts and less in others. As well, the data sets are scaled differently, but agreement is clearly displayed.

Similar trends are seen in the results for the 0.84% *b* gap height (Fig. 13). In the case of the stationary endwall, the cross-tip pressure gradients become visible at around 55% C_{ax}, further downstream than the case with twice the gap height. However, the C_P values are significantly higher for this smaller gap. The higher C_p values are also closer to the tip gap entrance for this gap height, giving evidence of a smaller flow separation region for the smaller gap clearance. Similar to the larger gap case, the cross-tip velocity gradients appear further downstream with the endwall motion. The pressure fields appear to be similar, with and without motion in the downstream part of the blade.

The smallest gap case, 0.56% *b*, also displays similar trends as the other two flat tip cases (Fig. 14). Again, the relative endwall motion is seen to lower the velocities in the front part of the blade and push back the high cross-tip velocity gradients. Continuing the trend of decreasing gap, the high cross-tip velocities are seen to be closer to the pressure side and not visible in moving endwall case, due to limits in the measurement area.

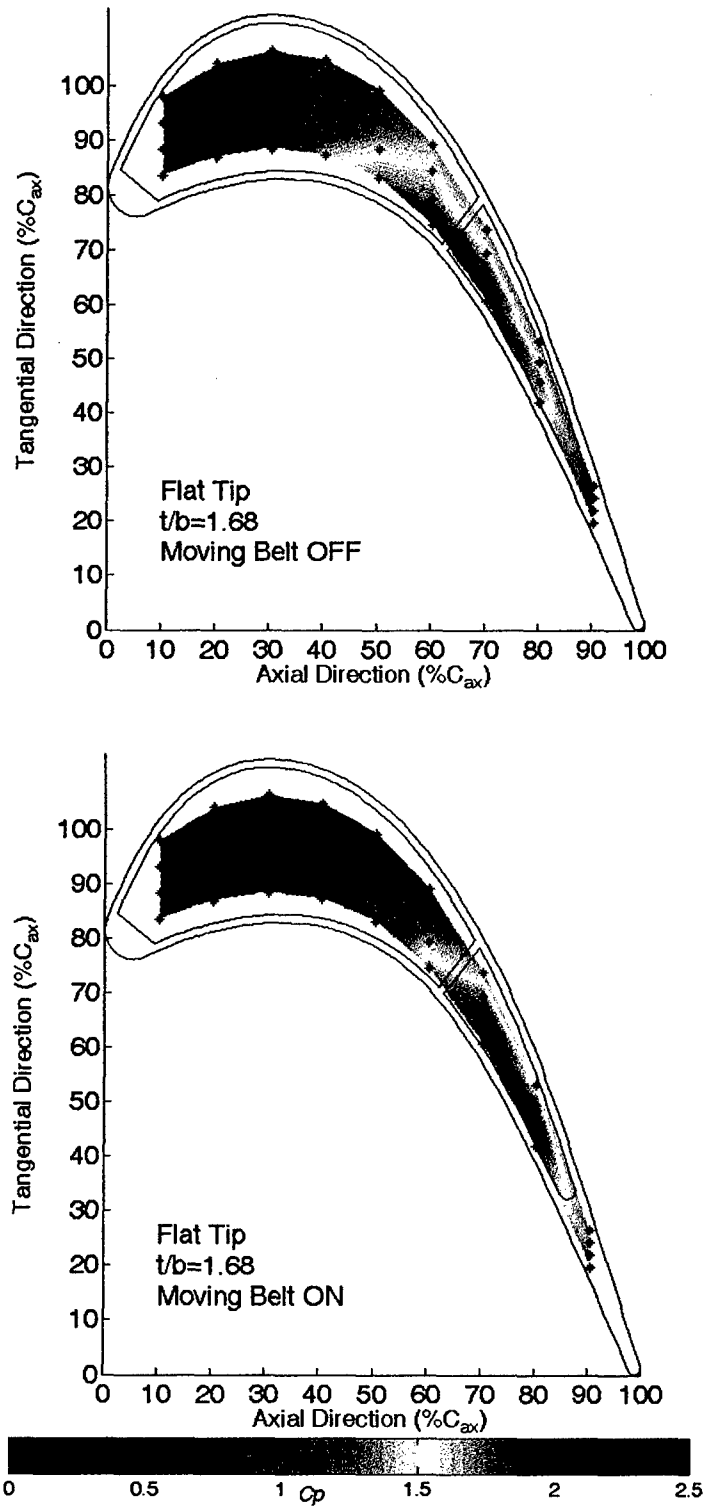

Fig. 12 C_P distribution for flat tip with t/b= 1.68%.

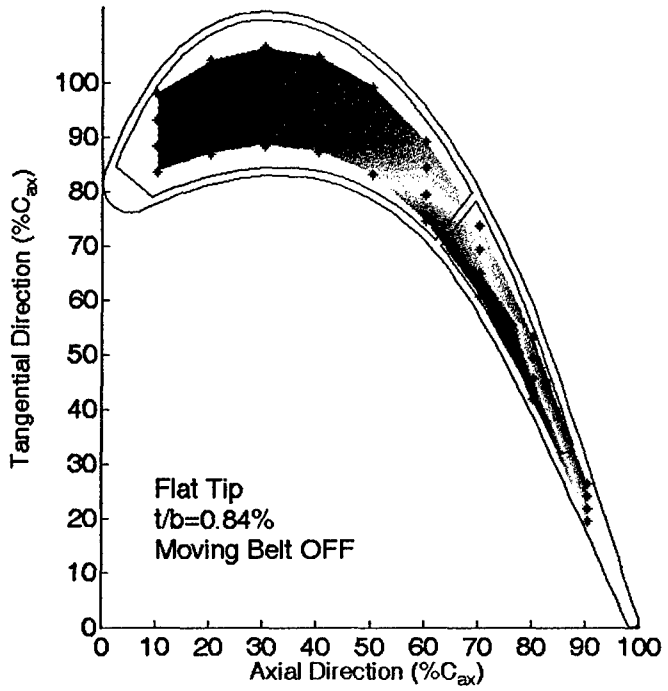

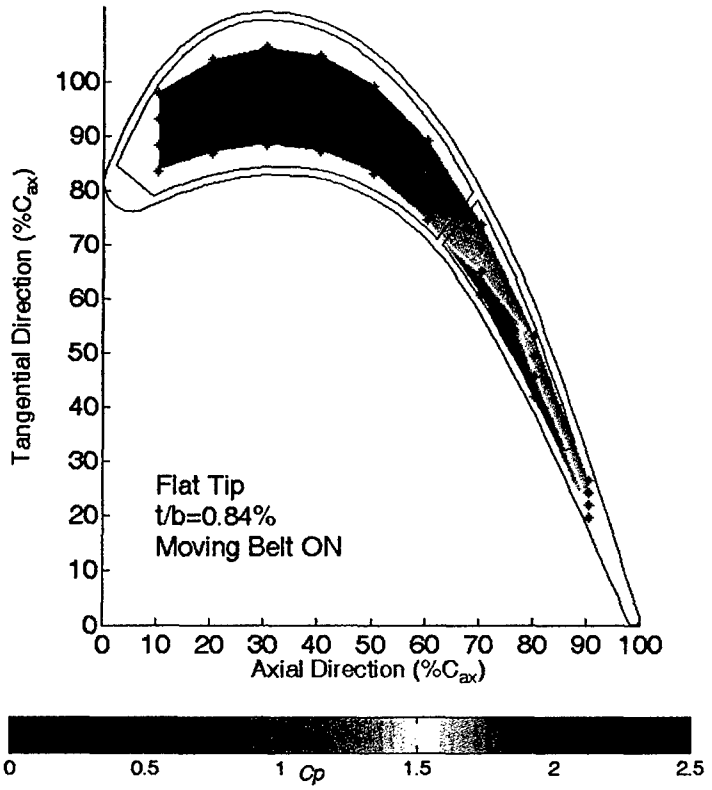

Fig. 13 C_P distribution for flat tip with t/b=0.84%.

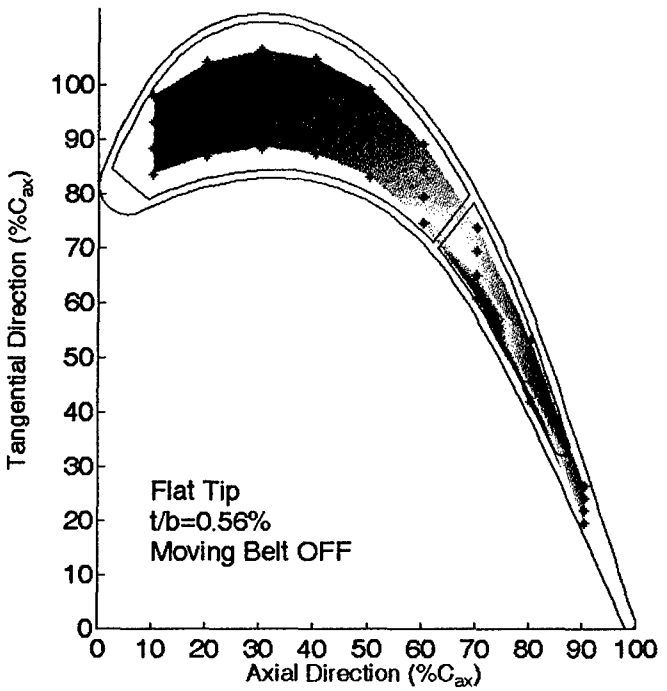

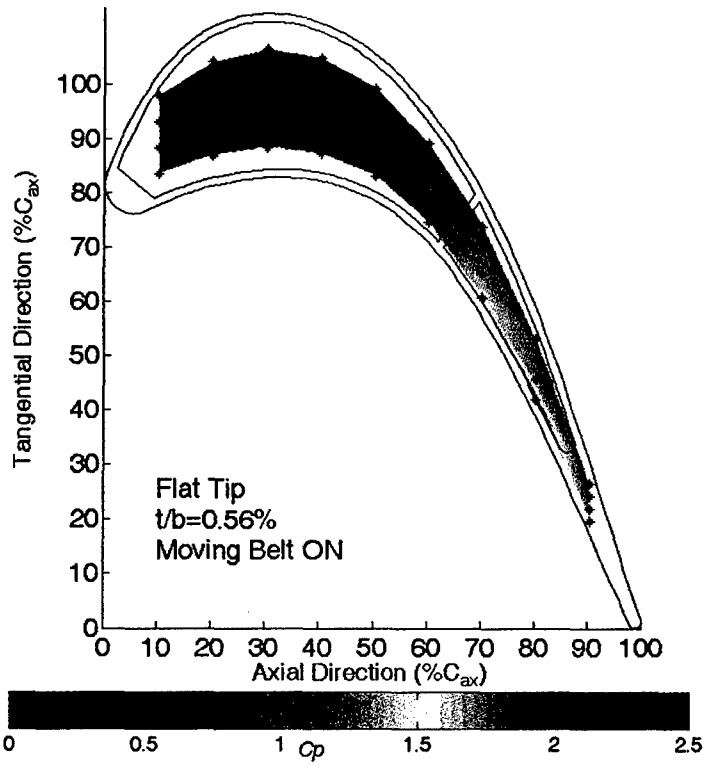

Fig. 14 C_P distribution for flat with t/b= 0.56%.

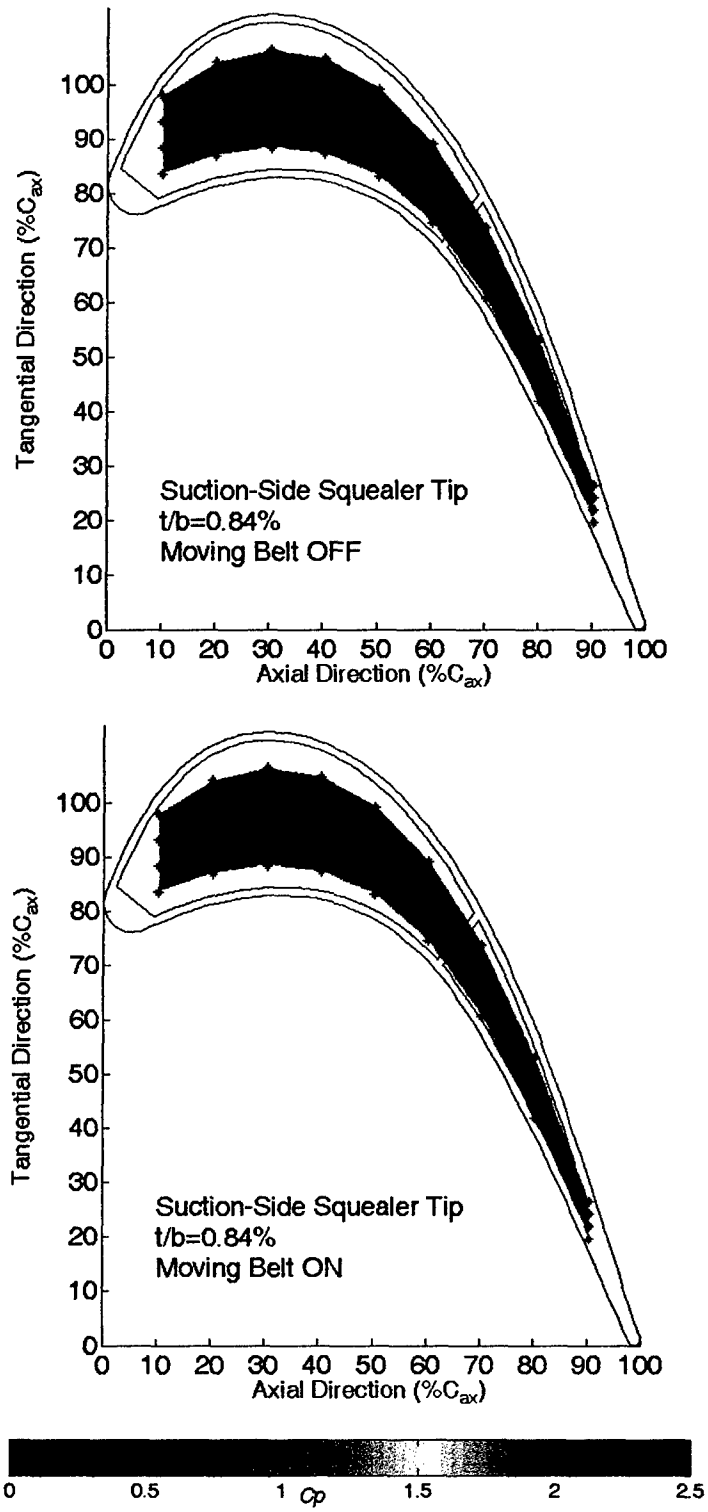

Fig. 15 C_P distribution for Suction-Side Squealer tip with t/b= 0.84%.

Tip pressure measurements for the suction side squealer tip geometry are shown in Fig. 15, for a tip gap 0.84% *b*. The tip results reveal the suction side squealer has the lowest tip gap velocities inferred of all the cases tested, as is expected. Similar to the other cases, the C_P is higher as you move downstream of the blade. Also, the higher velocities are found near the pressure side of the tip, decreasing as the flow approaches the suction side of the tip where it meets the squealer on the suction side and exits onto the passage.

Pressure Profiles

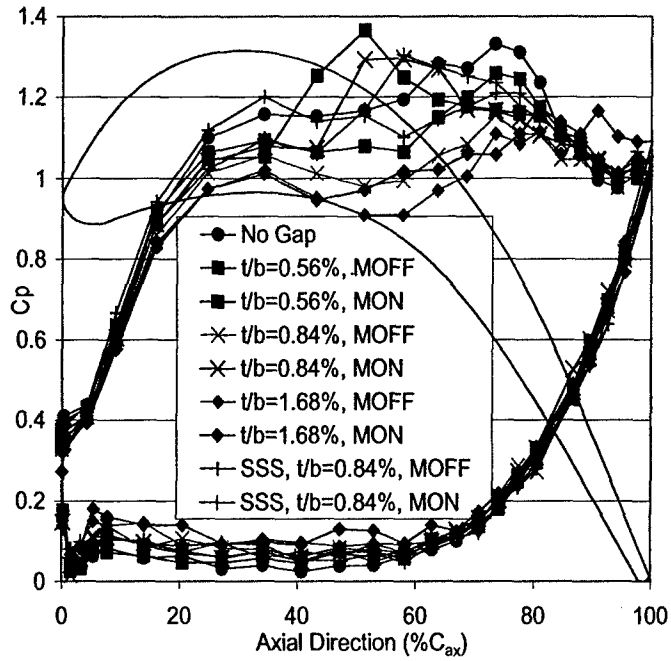

Fig. 16 Airfoil Pressure distributions at 10%*C* from tip.

Airfoil pressure measurements for all the cases studied are presented in Fig. 16 for a spanwise location of 10% *C* from the blade tip. The profile of the case with no gap is also presented. The plots reveal the effect of the relative motion, gap clearance and tip geometry on the airfoil pressure distribution. However, at this location the pressures are also influenced by the neighboring secondary flow, tip leakage and passage vortex, well within this region as seen in [34]. For all cases, the pressure side pressures don't seem to vary very much from no gap case. Interestingly enough, the pressure on the suction side is reduced by the moving endwall and this region of lower pressure is pushed closer to the front of the blade, especially for the 0.56% *b* gap, creating a larger pressure gradient across the tip to drive the flow. This effect seems to decrease with increasing gap height. These results for the 1.68% *b* gap agree with the velocity measurements taken in the perpendicular planes in Fig. 9, Fig. 10 and Fig. 11 where the flow can be seen to have slightly higher velocities in the case of the moving endwall.

Nusselt Numbers on Blade Tip

Maps of Nusselt numbers (*Nu*) on the blade tip surface for the cases tested are presented in the following figures. *Nu* is defined by Equation 3. If the reader wishes to extract *h* values from these maps, the axial chord is length is equal to 808 mm and the thermal conductivity of the fluid is defined as 26.3 x 10^{-3} $Wm^{-1}K^{-1}$. So that $h = Nu*(0.0326)$

$Wm^{-2}K^{-1}$. Similarly, if Stanton numbers are desired, Equation 4 can be used to give $St = Nu*(3.536*10^{-6})$.

$$Nu = \frac{hC_{ax}}{k_f} \qquad (3)$$

$$Nu = StRePr \qquad (4)$$

The *Nu* maps cover most the tip region surface area. The maps are superimposed onto the blade profile to give a clear indication of where the data is found. Thermocouples used to measure the temperature at three locations on the test surface are also displayed on the maps and can easily be distinguished. Flow measurements already presented help to understand the heat transfer results in this section. All maps are plotted to the same scale for ease of comparison.

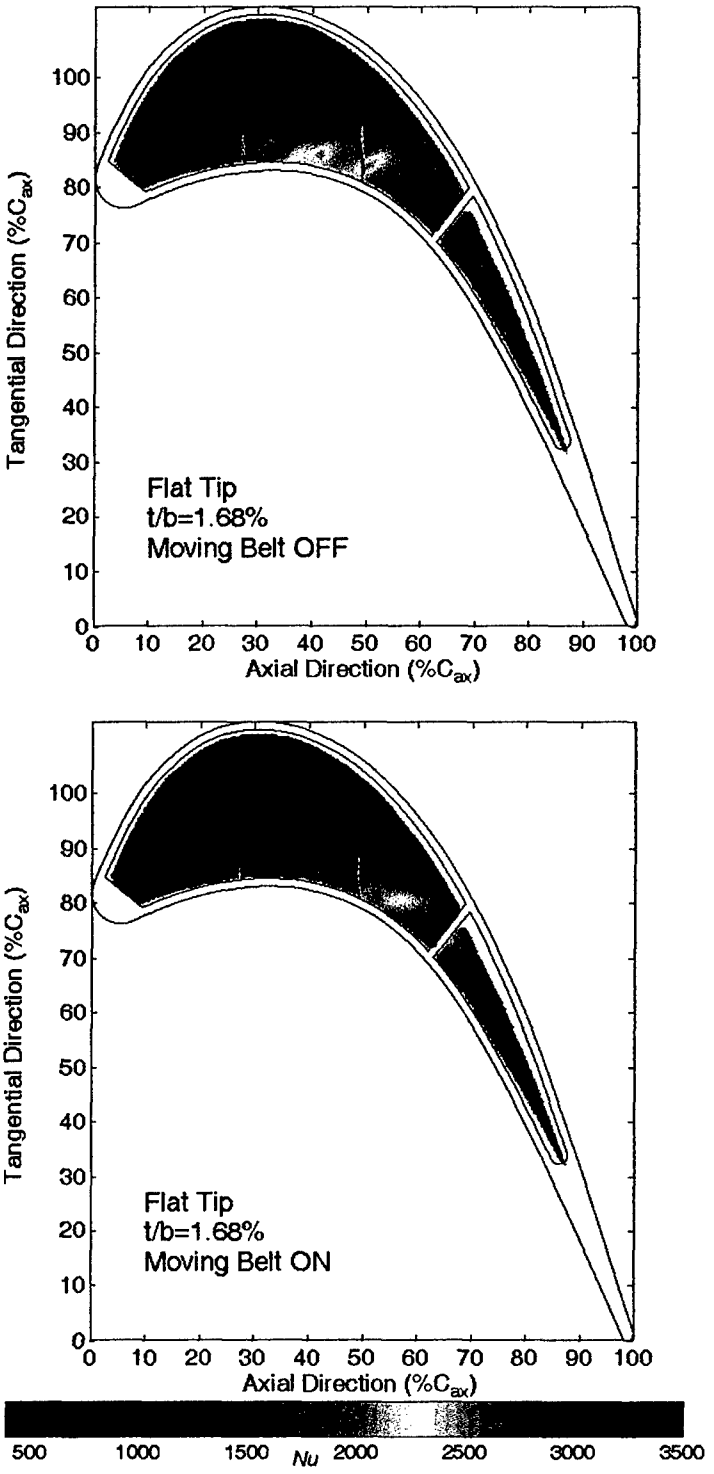

Fig. 17 *Nu* Map for flat tip with *t/b*= 1.68%.

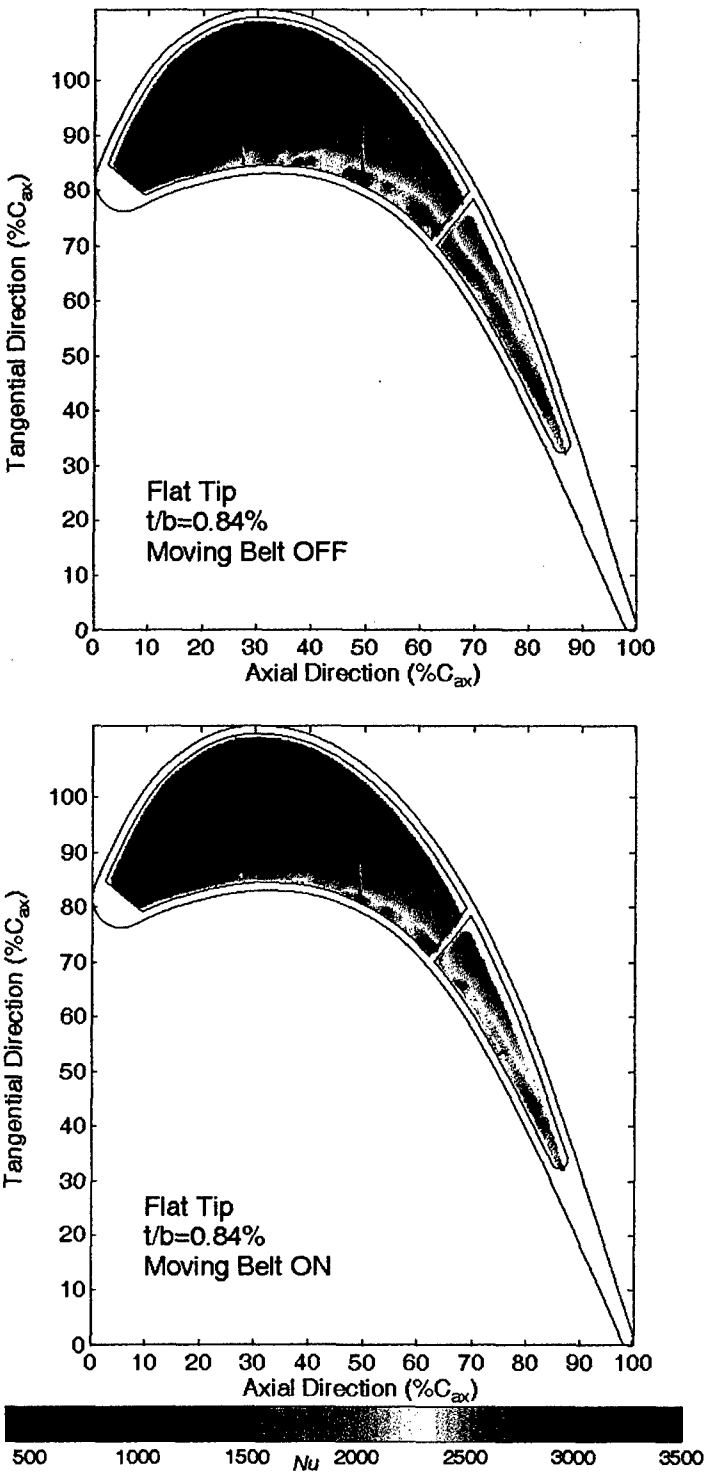

Fig. 18 *Nu* Map for flat tip with *t/b*= 0.84%.

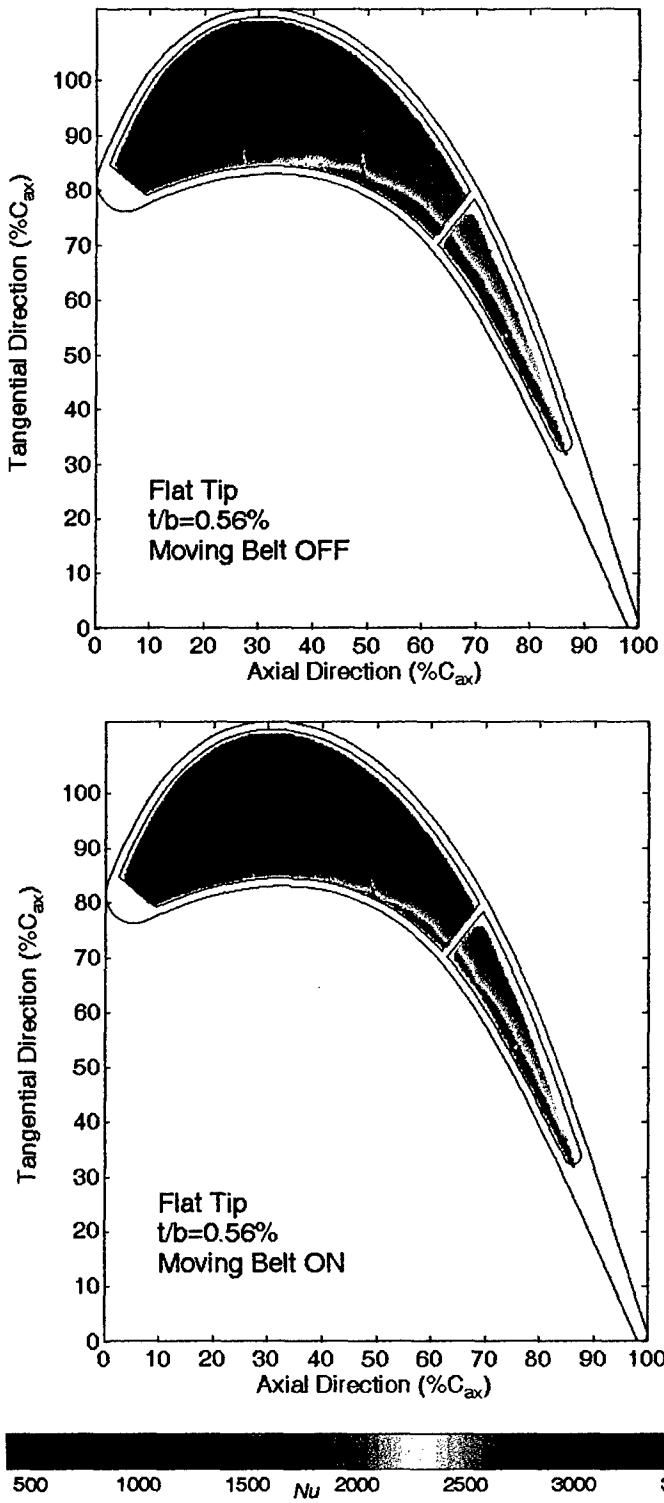

Fig. 19 *Nu* Map for flat tip with *t/b*= 0.56%.

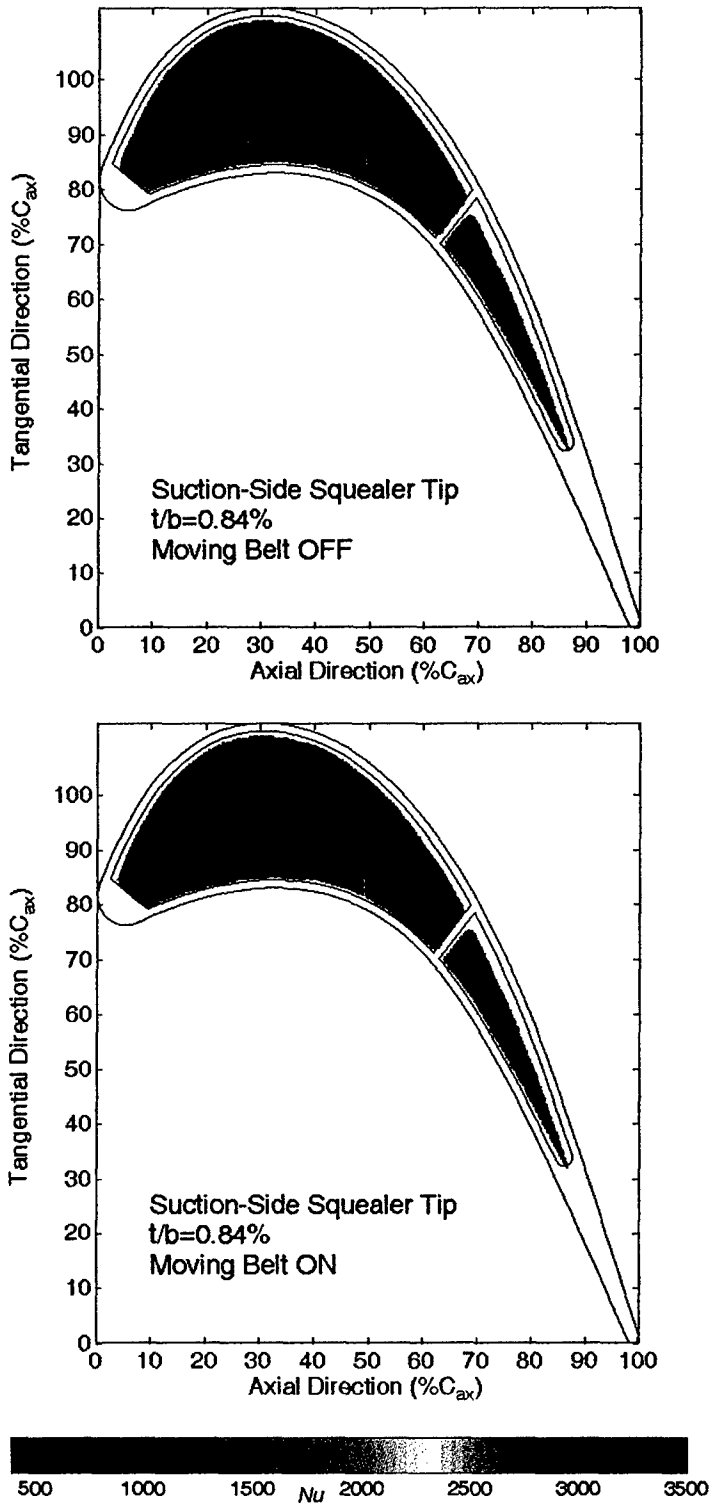

Fig. 20 *Nu* Map for Suction-Side Squealer with *t/b*= 0.84%.

All *Nu* maps display a low heat transfer region in the front part of the blade near the crest, referred to as the sweet spot in [40]. It can be seen how the thermal boundary layer develops at the leading edge of the blade and *Nu* decreases as the flow moves down the blade in a direction close to the inlet angle.

For the case of 1.68% *b* gap (Fig. 17), higher *Nu* levels are visible from approximately 40% C_{ax} onward for the

stationary endwall case. These high *Nu* regions coincide with the lower C_P levels that follow from the region of high C_P near the pressure side edge for this case, shown in Fig. 12. In the latter part of the blade, the high C_P levels extend further into the gap and the higher *Nu* levels appear closer to the suction side edge. The high *Nu* values are most likely associated with the reattachment of the flow. Looking at the case with moving endwall, the high *Nu* values have lessened and have moved further downstream from the front part of the blade. The location where the blade material divides the data into two parts shows high *Nu* values, which coincide with the location of the perpendicular plane 63.5 cm from the TE (Fig. 9). In the perpendicular plane, it can be seen that the separation bubble is reduced by the moving endwall motion and the flow thus reattaches earlier in the gap, which can be associated with the high *Nu* values found here. The tip pressures in Fig. 12 also show this location to have high velocity gradients where the high velocity region becomes evident slightly beforehand and the high velocity covers most of the tip width after this region, showing signs of no reattachment in the latter part of the blade.

The plots for 0.84% *b* (Fig. 18) show higher *Nu* values than those with twice the gap size; similar results were found in [39]. The highest *Nu* values, depicted by reddish color, are more noticeable and appear to be closer to the tip pressure side edge. This agrees with the tip pressure results where the values of C_P are higher for the smaller gap than for the larger gap. As in the larger gap case, the effect of the moving endwall also pushes the higher *Nu* regions further downstream of the blade. However, the *Nu* distributions seem similar for both cases of endwall motion in the latter part of the blade. This agrees with the tip pressures where the distributions of C_P are similar for both cases of endwall motion in the latter part of the blade.

The results for the 0.56% *b* gap (Fig. 19) revealed high *Nu* values concentrated even closer to the tip pressure side edge. The moving endwall again pushes the high *Nu* regions further downstream and closer to the pressure side. In Fig. 14 the region of high C_P is just visible near the pressure side for stationary endwall case. For the moving endwall, the high C_P region is almost completely unseen in the measurements, suggesting the higher velocity regions are very close to the pressure side.

The plot for the suction–side squealer tip with 0.84% *b* gap is presented in Fig. 20. It can be seen that the suction squealer tip geometry case has the lowest heat transfer out of all the cases. The sweet spot, the lowest heat transfer region, is still present for this geometry. The highest *Nu* values are about less than twice the highest values of the other cases, showing the advantage of this geometry. This is supported by the measurements of C_P in Fig. 15, where the levels were less than twice the amounts of those for the flat tip cases.

Overall averaged *Nu* values for stationary endwall cases were 1247, 1357, 1196 and 914 for the flat tip with 0.56% *b*, 0.84% *b*, and 1.68% *b* gaps and the suction-side squealer tip with 0.84% *b*, respectively. For the flat tip cases, reductions in averaged *Nu* due to the moving endwall effect were measured to be 13.3%, 12.45%, and 7.5% for the 0.56% *b* gap, 0.84% *b* gap, and 1.68% *b* gap, respectively. For the suction-side squealer tip, an increase of 1.75% in averaged *Nu* was measured due to the moving endwall effect. An incredible 32% reduction in *Nu* was seen with the inclusion of the suction-side squealer tip for the 0.84% *b* gap.

Uncertainty Analysis of h

The typical uncertainty in the measurement of the heat transfer coefficients was of 5.1% (Table 5), with a very small range getting up to 12.2%.

Table 5 Typical Uncertainty for *h*

Measurement	Typical value	Standard error	Contribution to uncertainty in heat transfer coefficient.
Current	4.5 A	0.050 A	0.6732 $Wm^{-2}K^{-1}$
Voltage	27.37 V	0.2737 V	0.6059 $Wm^{-2}K^{-1}$
Area	0.145 m^2	0.00145 m^2	0.6058 $Wm^{-2}K^{-1}$
Typical surface temp	35°C	0.5 °C	2.181 $Wm^{-2}K^{-1}$
T gas	21 °C	0.3 °C	1.288 $Wm^{-2}K^{-1}$
Emissivity	1.08	0.05	0.3094 $Wm^{-2}K^{-1}$
Root mean square total	-	-	2.775 $Wm^{-2}K^{-1}$ = 5.2%

CONCLUSIONS

A very large-scale linear, 3-passage cascade has been used to produce representative flow conditions around a central blade. The scale of the setup has enabled uniquely detailed heat transfer, PIV and pressure measurements on the tip surface and of the over-tip leakage flows. This detail was possible due to the large tip gaps (up to 30 mm) employed. The relative motion between the turbine casing and rotor blade has been simulated with a moving belt.

The separation bubble under the tip has been clearly characterized, revealing its significant effect on the leakage flow. The moving endwall had a clear influence on the shape and size of the separation bubble and associated velocities and heat transfer at certain locations for the gaps investigated. For example, at the examined plane close to the mid-axial chord, the bubble was reduced to approximately half of its height from the case without endwall movement. This effect was less in the further downstream locations, but increases in velocities were measured for the relative endwall motion cases.

Tip pressure measurements provided great insight to the tip leakage flow behavior. Compared with previous mid-gap plane PIV measurements, the tip pressure measurements supported the effect of the moving endwall on the tip leakage flow. The velocity of the flow was weakened by the moving endwall in the front part of the blade. Regions of high velocity and high cross-tip velocity gradients revealed the effect of the flow separation at the pressure side of the tip gap. These high velocity regions are seen to be shifted by the moving endwall effect. Further downstream, near the trailing edge, the velocities are largely unaffected by the relative endwall motion. Higher cross-tip velocities were measured

for the smaller gaps. The suction-side squealer tip showed significantly lower velocities than the flat tip cases.

High resolution *Nu* maps revealed characteristics reported in previous studies, i.e. the low heat transfer region near the crest and the high heat transfer regions near the pressure side. Higher *Nu* values were measured for the smaller tip gap case. The moving endwall altered the location of the high heat transfer region. Further downstream, the local heat transfer was not significantly affected by the moving endwall. The suction side squealer tip geometry showed significantly lower local *Nu* values in comparison to the flat tip cases. Averaged *Nu* values for the flat tip cases were seen to be higher for the smaller gaps. The suction-side squealer tip showed the lowest averaged *Nu* values, resulting in a 32% reduction in the overall average *Nu*. The relative endwall motion reduced the overall averaged *Nu* by a maximum of 13.3%.

Further PIV and heat transfer studies for different gap heights and tip geometries, together with the unsteadiness of the over-tip flow field, are underway.

ACKNOWLEDGMENTS

This work is supported by the Air Force Office of Scientific Research under Grant F49620-02-0027 with Thomas Beutner as the technical officer. Their support is greatly appreciated. The authors also wish to extend their gratitude to Mr. Trevor Godfrey for his useful suggestions and contributions to the design, assembly and manufacturing of the experimental setup.

REFERENCES

[25] Booth, T. C., Dodge, P. R., Hepworth, H. K., 1982. "Rotor-Tip Leakage: Part 1 – Basic Methodology," ASME Journal of Engineering for Power, Vol. 104, pp. 154-161.

[26] Hirsch, C., (Ed.) AGARD-AG-328, 1993. "Advanced Methods for Cascade Testing."

[27] Moore, J., Tilton, J. S., 1987. "Tip Leakage Flow in a Linear Turbine Cascade," ASME Paper 87-GT-222.

[28] Heyes, F. J. G., Hodson, H. P., 1991. "The Effect of Blade Tip Geometry on the Tip Leakage Flow in Axial Turbine Cascades," ASME Paper 91-GT-135.

[29] Bindon, J. P., 1987. "Pressure Distributions in the Tip Clearance Region of an Unshrouded Axial Turbine as Affecting the Problem of Tip Burnout," ASME Paper 87-GT-230.

[30] Bindon, J. P., 1989. "The Measurement and Formation of Tip Clearance Loss," Journal of Turbomachinery, Vol. 111, pp. 257-263.

[31] Yaras, M. I., Sjolander, S. A., 1992. "Prediction of Tip-Leakage Losses in Axial Turbines," Journal of Turbomachinery, Vol. 114, pp. 204-210.

[32] Yaras, M. I., Sjolander, S. A., 1991a. "Effects of Simulated Rotation on Tip Leakage in a Planar Cascade of Turbine Blades, Part I: Tip Gap Flow," ASME Paper 91-GT-127.

[33] Yaras, M. I., Sjolander, S. A., Kind, R. J., 1991b. "Effects of Simulated Rotation on Tip Leakage in a Planar Cascade of Turbine Blades, Part II: Downstream Flow Field and Blade Loading," ASME Paper 91-GT-128.

[34] Palafox, P., Oldfield, M.L.G., Jones, T.V. and LaGraff, J., 2005, "PIV Maps of Tip Leakage and Secondary Flow Fields On a Low Speed Turbine Blade Cascade with Moving Endwall," ASME Paper GT2005-68189.

[35] Yamamoto, A., 1988. "Interaction Mechanisms Between Tip Leakage Flow and the Passage Vortex in a Linear Turbine Rotor Cascade," Journal of Turbomachinery, Vol. 110, pp. 329-338.

[36] Yamamoto, A., 1989. "Endwall Flow/ Loss Mechanisms in a Linear Turbine Cascade with Blade Tip Clearance," Journal of Turbomachinery, Vol. 111, pp. 264-274.

[37] Mayle, R. E., Metzger, D. E., 1982. "Heat Transfer at the Tip of an Unshrouded Turbine Blade," Proc., Seventh Int. Heat Transfer Conference, Vol. 3, pp. 87-92.

[38] Chyu, M. K., Moon, H. K. Moon, Metzger, D. E., 1989. "Heat Transfer in the Tip Region of Grooved Turbine Blades," ASME Journal of Turbomachinery, Vol. 111. pp. 131-138.

[39] Srinivasan, V., Goldstein, R. J., 2003. "Effect of Endwall Motion on Blade Tip Heat Transfer," ASME Journal of Turbomachinery, Vol. 125, pp. 267-273.

[40] Bunker, R. S., Bailey, J. C., Ameri, A. A, 2000. "Heat Transfer and Flow on the First-Stage Blade Tip of a Power Generation Gas Turbine: Part 1 – Experimental Results," ASME Journal of Turbomachinery, Vol. 122, pp. 263-271.

[41] Azad, G. S., Han, J. C., Teng, S., 2000. "Heat Transfer and Pressure Distributions on a Gas Turbine Blade Tip," ASME Paper 2000-GT-194.

[42] Chana, K. S., Jones, T. V., 2002. "An Investigation On Turbine Tip and Shroud Heat Transfer," ASME Paper GT-2002-30554.

[43] Thorpe, S. J., Yoshino, S., Ainsworth, R. W., Harvey, N. W., 2004. "An investigation of the heat transfer and static pressure on the over-tip casing wall of an axial turbine operating at engine representative flow conditions (I) Time-mean results," Int. Journal of Heat and Fluid Flow, Vol. 25, pp. 933-944.

[44] Thorpe, S. J., Yoshino, S., Ainsworth, R. W., Harvey, N. W., 2004. "An investigation of the heat transfer and static pressure on the over-tip casing wall of an axial turbine operating at engine representative flow conditions (II) Time-resolved results," Int. Journal of Heat and Fluid Flow, Vol. 25, pp. 945-960.

[45] Greenway, M.E. and Wood, C. J., 1979, "The Oxford University 4 m x 2 m Industrial Aerodynamic Wind Tunnel," Journal of Industrial Aerodynamics, Dept. of Engineering Science, University of Oxford.

[46] Gregory-Smith, D. G., Cleak, J. G. E., 1992, "Secondary Flow Measurements in a Turbine Cascade with High Inlet Turbulence," ASME Journal of Turbomachinery, Vol. 114, pp.173-183.

[47] Keane, R. D. and Adrian, R. J., 1992. "Theory of Cross-correlation Analysis of PIV images," Appl. Sci. Res. 49, pp. 1-27.